Aus dem Insitut für Pathologie
(Prof. Dr. med. P. Ströbel)
der Medizinischen Fakultät der Universität Göttingen

Regulation and therapeutic targeting of MTHFD2 and EZH2 in KRAS mutated human pulmonary adenocarcinoma

INAUGURAL-DISSERTATION

zur Erlangung des Doktorgrades
der Medizinischen Fakultät der
Georg-August-Universität zu Göttingen

vorgelegt von

Yuchan Li

aus
Guangzhou, Guangdong, China

Göttingen 2023

Dekan: Prof. Dr. med. W. Brück

Betreuungsausschuss

Betreuer*in: Prof. Dr. med. P. Ströbel

Ko-Betreuer*in: PD Dr. med. A. von Hammerstein-Equord

Prüfungskommission

Referent*in: Prof. Dr. med. P. Ströbel

Ko-Referent*in:

Drittreferent*in:

Datum der mündlichen Prüfung: ……

Hiermit erkläre ich, die Dissertation mit dem Titel „Regulation and therapeutic targeting of MTHFD2 and EZH2 in KRAS mutated human pulmonary adenocarcinoma“ eigenständig angefertigt und keine anderen als die von mir angegebenen Quellen und Hilfsmittel verwendet zu haben.

Göttingen, den …… ……

(Unterschrift)

Die Daten, auf denen die vorliegende Arbeit basiert, wurden teilweise publiziert:

Publication 1: **Li Y**, Elakad O, Yao S, von Hammerstein-Equord A, Hinterthaner M, Danner BC, Ferrai C, Ströbel P, Küffer S, Bohnenberger H (2022): Regulation and Therapeutic Targeting of MTHFD2 and EZH2 in KRAS-Mutated Human Pulmonary Adenocarcinoma. Metabolites 12, 652

Publication 2: Elakad O*, **Li Y***, Gieser N*, Yao S, Küffer S, Hinterthaner M, Danner BC, von Hammerstein-Equord A, Ströbel P, Bohnenberger H (2021): Role of Annexin A1 in Squamous Cell Lung Cancer Progression. Dis Markers 2021, 5520832

*equal contribution

Publication 3: Tirilomi A, Elakad O, Yao S, **Li Y**, Hinterthaner M, Danner BC, Ströbel P, Tirilomis T, Bohnenberger H, von Hammerstein-Equord A (2022): Expression and prognostic impact of CD49b in human lung cancer. Medicine (Baltimore) 101, e28814

Table of Contents

List of Figures

List of Tables

Abbreviations

AC	Adeno carcinoma
ALK	Anaplastic Lymphoma Kinase
ATCC	American type culture collection
1CM	one-carbon metabolism
CC BY 4.0	Creative Commons Attribution-ShareAlike 4.0
CRC	Colorectal cancer
DMSO	Dimethyl sulfoxide
DNA	Deoxyribonucleic acid
EDTA	Ethylene diamine tetraacetic acid
EGFR	Epidermal growth factor receptor
ERK	Extracellular signal regulated kinases
E. coli	Escherichia coli
EZH2	Enhancer of Zeste Homolog 2
FBS	Fetal bovine serum
FCS	Fetal calf serum
FDA	Food and drug administration
GAPDH	Glyceraldehyde 3-phosphate dehydrogenase
gRNA	Guide RNA
H3K27me3	Histone 3 lysine 27 trimethylation
IC50	Half maximal inhibitory concentration
IHC	Immunohistochemistry
KRAS	Kirsten rat sarcoma viral oncogene homologue
LC	Lung cancer
MEK	Mitogen activated protein kinase kinase
MTHFD2	Methylenetetrahydrofolate dehydrogenase 2
NSCLC	Non-small cell lung cancer
OS	Overall survival
PARK7	Parkinsonism Associated Deglycase
PBS	Phosphate buffered saline
PCR	Polymerase chain reaction
PFS	prolonged progression-free survival
PTX	Pemetrexed
RNA	Ribonucleic acid
RPM	Revolutions per minute
RPMI	Roswell Park Memorial Institute
RT	Room temperature
SCLC	Small cell lung cancer
SDS	Sodium dodecyl sulfate

siRNA	Small interfering RNA
SQCLC	Squamous cell lung cancer
Taq	Thermus aquaticus
TBE	Tris/borate/EDTA
TKI	Tyrosine kinase inhibitor
TBST	Tris buffered saline with Tween 20
UMG	University Medical Center Göttingen
Western blotting	WB
WT	Wild type

1 Introduction

1.1 Lung cancer

1.1.1 Epidemiology and Mortality

With a five-year survival rate of 10 % to 20 %, lung cancer (LC) is one of the most aggressive and deadliest cancer types, with the highest cancer-related death rate in men and, after breast cancer, the second highest mortality in women (Sung et al. 2021). Statistically, there were almost 2.2 million new cases and 1.8 million deaths worldwide in 2020, accounting for about 11.4 % of identified cancers and 18.0 % of total cancer deaths. Smoking is the main risk factor and accounts for 85 % to 90 % of all lung cancer cases (Schwartz and Cote 2016). Cancer substances in tobacco smoke can activate deoxyribonucleic acid (DNA) sequence damages that favor the development of lung cancer (Hecht 1999). Exposure to secondhand smoke can also increase the risk of lung cancer in non-smokers (Kim et al. 2015; Öberg et al. 2011). Patients with pulmonary tuberculosis (Brenner et al. 2016) and chronic obstructive pulmonary disease (COPD) (Brenner et al. 2012; Turner et al. 2007) also have an increased incidence of lung cancer.

1.1.2 Histological classification

Lung cancer mainly originates from bronchial mucinous glands, alveoli, bronchial epithelium, and bronchioles. Many studies have shown that lung cancer is caused by a series of pathological changes (Cho and Vogelstein 1992; Wistuba et al. 1999). Histologically, lung cancer is classified into two main groups, non-small cell lung cancer (NSCLC) with an occurrence of about 85 % (Duruisseaux and Esteller 2018; Sung et al. 2021) and small cell lung cancer (SCLC) with 15 % of all diagnosed cases. NSCLC are further divided into Adenocarcinoma (AC) and Squamous cell carcinoma (SQCLC) (Travis et al. 2015). Among all types of lung cancer, SCLC is the most aggressive with a rapid progression and poor prognosis (Rodriguez-Canales et al. 2016; Zheng 2016). AC is the most frequent type of NSCLC, accounting for about 40 % of lung cancer (Figure 1) (Sung et al. 2021; Travis et al. 2015).

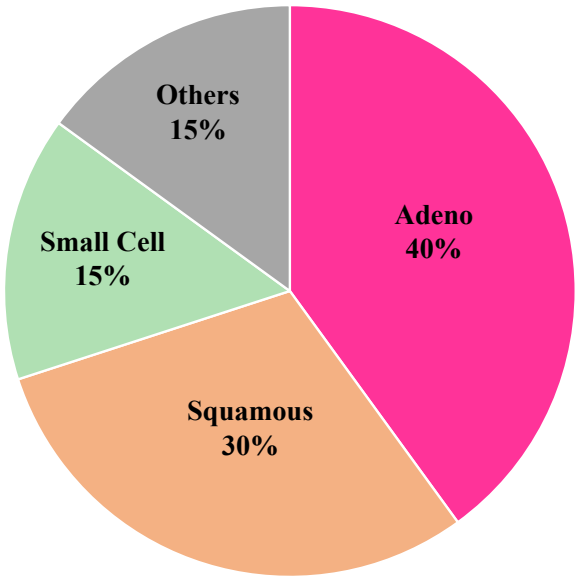

Figure 1: Distribution of histological subtypes of Lung Cancer.

1.2 Therapeutic Strategies of NSCLC

To achieve the best response and possible cure for early-stage NSCLC, the decision for a local (surgery or radiotherapy) or related systemic treatment is a matter of multidisciplinary discussion. In addition, consensus guidelines support cisplatin-based adjuvant therapy that supports surgical cancer resection or is administered concurrently with radiotherapy (Ettinger et al. 2022). Unfortunately, NSCLC is not obvious in its early stages, so it does not produce any symptoms until the disease progresses. With effective trial designs and a growing focus on advanced diseases, newer agents (currently the standard of care for patients with stage IV disease) have been incorporated into the therapeutic paradigm of radical treatment. Surrogate endpoints, such as pathological response and immunotherapy combined with targeted therapy, are under investigation and may shorten the trial duration. Encouragingly, Durvalumab, a potential anti-PD-L1 antibody, was approved in 2018 for the treatment of lung cancer patients (stage III) after concurrent chemoradiotherapy (Chaft et al. 2021).

1.3 Molecular subtypes and therapeutic strategies in NSCLC

Histological differentiation and (Tumor, node and metastasis system) TNM stage cannot differentiate between molecular subtypes and possible requirements of individualized and precise prognostic evaluation of NSCLC. Transcriptomics, genomics, proteomics and epigenomics have revealed molecular subtype classifications of NSCLC (El Osta et al. 2019; Guibert et al. 2015) that opened the opportunity for target-specific strategies and precision

treatment of patients (Fujimoto et al. 2016; Weller et al. 2015; Woo et al. 2017; Xu et al. 2019) (Figure 2).

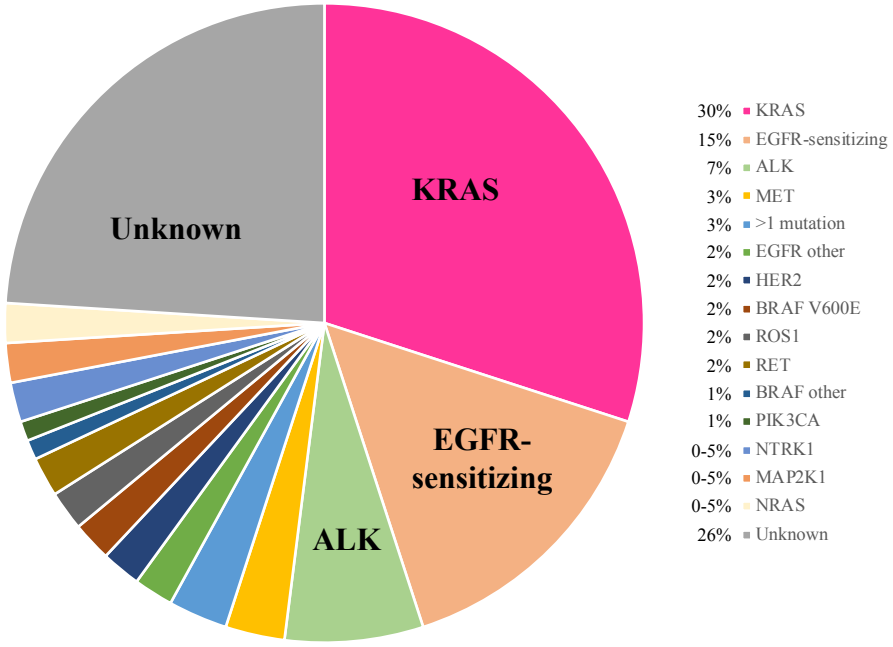

Figure 2: Distribution of molecular subtypes in AC.

With the discovery of molecular targets and the increasing availability of specific target agents, treatment options for lung adenocarcinoma have changed dramatically over the last decade (Pan et al. 2019). For advanced NSCLC patients with epidermal growth factor receptor (EGFR) activating mutations (17 % of all AC cases), treatment with tyrosine kinase inhibitors (TKI) has resulted in significantly prolonged progression-free survival (PFS) and overall survival (OS) in comparison to standard platinum-based chemotherapy (Lindeman et al. 2013). However, secondary resistance mutations can occur in patients treated with TKI and new treatment options are needed to maintain the therapeutic effect (Sequist et al. 2013; Yu et al. 2013). NSCLC patients with c-ROS oncogene 1 (ROS1) or anaplastic lymphoma kinase (ALK) rearrangements have been shown to respond well to crizotinib as another TKI (Addeo et al. 2018; Friedlaender et al. 2019), and advanced NSCLC patients harboring v-raf murine sarcoma viral oncogene homolog B (BRAF) p.V600E mutations benefit from the combinational therapy with the BRAF inhibitors dabrafenib and trametinib (Frisone et al. 2020; Planchard et al. 2017; Planchard et al. 2016). For a long time, Kirsten rat sarcoma viral oncogene homologue (KRAS) mutated tumors, which is the largest molecular subgroup in AC with a prevalence of 30 % were considered to be undruggable (Figure 2). The discovery

of the KRAS G12C ($KRAS^{G12C}$) specific inhibitor AMG510 (Sotorasib) also made this defined molecular subgroup treatable. Sotorasib was approved by the Food and Drug Administration (FDA) in 2021 for second-line treatment of AC patients. In addition, the potent covalent $KRAS^{G12C}$ inhibitor Adagrasib (MRTX 849) is being evaluated by the FDA as a therapy option for patients with previously treated $KRAS^{G12C}$-mutated NSCLC (Jänne et al. 2022). However, other KRAS mutations are non-targetable yet and the general response level for Sotorasib and Adagrasib among $KRAS^{G12C}$ cases stays lower than expected, with an average of around six out of ten patients evading response (Hong et al. 2020; Jänne et al. 2022; Nakajima et al. 2022; Skoulidis et al. 2021; Zheng et al. 2022). The American Society of Clinical Oncology (ASCO) recommends routine driver gene testing for EGFR, ALK, BRAF, ROS1, and KRAS in patients with metastatic NSCLC in clinical practice.

1.4 KRAS and one-carbon metabolism in AC

KRAS activating mutations define with 30 % of the largest subgroup of AC (El Osta et al. 2019; Guibert et al. 2015), and they are more common in AC than in all other NSCLC subtypes (Kalemkerian et al. 2018) (Figure 2). Substitutions at the codons 12 and 13 of KRAS are the most frequent mutations and are observed in about 13 % of NSCLC in smokers (Friedlaender et al. 2020).

In recent years several cellular functions and pathways have been identified to be regulated by KRAS (Saliani et al. 2022; Yuan et al. 2018). Recently, Stine et al. (2022) reported that KRAS mutations play an essential role in regulating tumor metabolism, for instance, stimulating tumor cells to uptake glucose (Stine et al. 2022; Yang et al. 2020; Ying et al. 2012). Chemoresistance, tumor progression, and metastasis of several malignant tumors are closely connected to elevated aerobic glycolysis and a raising need for energy. (Hanahan and Weinberg 2011; Kaelin and Thompson 2010; Tao et al. 2014; Zhou et al. 2012). Some scholars have demonstrated that KRAS mutations are related to an increased dependency on the one-carbon metabolism (1CM) in NSCLC and colorectal cancer (CRC) (Ju et al. 2019; Moran et al. 2014; Yao et al. 2021). 1CM, including folate cycles and methionine, plays a vital role in maintaining cellular homeostasis, and the integration of the cell's nutritional status by catabolizing different carbon sources to obtain one-carbon (methyl) units (Ben-Sahra et al. 2016; Christensen and MacKenzie 2006). Cancer cells maintain their high proliferation rates by using these 1CM units for reductive metabolism, nucleotide synthesis, and methylation (Ducker and Rabinowitz 2017). It was also shown that methylenetetrahydrofolate dehydrogenase 2 (MTHFD2) is vital for the cellular viability of NSCLC cells and serves as a

positive prognostic disease marker in AC (Yao et al. 2021). MTHFD2, one of the crucial enzymes of 1CM, is highly expressed during embryonic development, however, is barely expressed in healthy adult tissues, suggesting a promising potential target for cancer therapy (Nilsson et al. 2014). Besides, high expression levels of MTHFD2 have been correlated with tumor poor prognosis and recurrence in a variety of solid and hematologic malignancies, and are involved in resistance to pemetrexed (PTX) and gemcitabine (Bonagas et al. 2022; Ju et al. 2019; Nilsson et al. 2014; Shang et al. 2021; Song et al. 2018; Sugiura et al. 2022; Yang et al. 2021; Yao et al. 2021; Yu et al. 2020).

1.5 Role of EZH2 in tumor progression

Enhancer of Zeste homolog 2 (EZH2) as a component of polycomb repressive complex 2 (PRC2) regulates gene transcription by methylating H3K27 to Histone 3 lysine 27 trimethylation (H3K27me3) as a repressive mark and plays a key role in maintaining cell identity. EZH2 is upregulated in multiple malignancies, including ovarian, prostate, breast cancers, and NSCLC (Kim and Roberts 2016; Li et al. 2017; Riquelme et al. 2016; Shan et al. 2019; Wang et al. 2020; Yu et al. 2019; Zingg et al. 2015). Hu et al. (2010) discovered a significant association between EZH2 overexpression and chemoresistance, and predicted poor prognosis for epithelial ovarian cancers with overexpression of EZH2; therefore, in recent years, the inhibition of EZH2 as a clinical target has been tested. The specific EZH2 inhibitor GSK126 has yet not reached clinical stages. However, EPZ-6438 (Tazemetostat) received accelerated FDA approval for follicular lymphoma in early 2020 and has been tested in a variety of solid tumors (Hoy 2020; Italiano 2020; Morschhauser et al. 2020).

Recent studies have indicated a connection between EZH2 expression, KRAS mutation, and metabolism. The EZH2 expression levels of cells with KRAS wild-type ($KRAS^{WT}$) were much lower than in $KRAS^{G12C}$ cells and were moderate in cells with other KRAS mutations (Riquelme et al. 2016). The $KRAS^{G12C}$ and $KRAS^{G12D}$ mutated cells preferentially regulate EZH2 expression through the MEK-ERK and PI3K/AKT signaling pathways, respectively, while $KRAS^{G12S}$ can regulate EZH2 expression via both signaling pathways (Riquelme et al. 2016). Moreover, EZH2 has also been revealed to promote metabolic reprogramming in glioblastomas and overexpression of EZH2 impacted mitochondrial oxidative capacity at a low level. There was a remarkable increase in glycolytic metabolism which was indicated by either the activities of pivotal enzymes involved in glycolysis and lactate production or cellular deoxyglucose uptake (Pang et al. 2016).

1.6 Aim of the Study

Lung cancer is one of the most aggressive and deadliest cancer types. With the increasing availability of mutation-specific targeted agents and immune therapies, therapeutic options for AC have changed dramatically over the last decade (Pan et al. 2019). Due to the high somatic mutation rate and genomic rearrangements in AC (Cancer Genome Atlas Research Network 2014), the role of combining molecular, genomic and metabolomic analysis in the diagnosis and therapy of lung adenocarcinoma is receiving increasing attention (Li et al. 2021).

The current thesis aimed to investigate the metabolic and epigenetic network in the context of aberrant KRAS activity in AC. The 1CM makers and potential therapeutic target MTHFD2 and the epigenetics factor EZH2 were chosen as representing factors in AC. Our specific objectives were as follows: The first part was to resolve EZH2 and MTHFD2 expression and prognostic impact in correlation with the KRAS mutation status in AC patient tissue samples. The second part was to investigate intrinsic metabolic and epigenetic networks regulated by aberrant KRAS in AC cells. Finally, therapeutic interventions against EZH2 and MTHFD2 in AC cell lines with KRAS mutations were evaluated.

2 Materials and Methods

2.1 Materials

2.1.1 Equipment

Table 1: Summary of equipment

Equipment	Suppliers
Autoclave	Systec VX 100
Bacterial incubator, Heraeus instruments function line	Thermo Fischer Scientific, Waltham, USA
Bacterial shaker, orbital shaker	VWR, Pennsylvania, USA
Eppendorf Centrifuge 5424	Eppendorf, Hamburg, Germany
Eppendorf Centrifuge 5430R	Eppendorf, Hamburg, Germany
Fusion Fx Vilber Lourmat	Vilber Lourmat Deutschland GmbH, Eberhardzell, Germany
Genetic analyzser 3500	Thermo, Fisher Scientific GmbH, Germany
Herasafe, biological culture hood, Heraeus instruments	Thermo Fischer Scientific, Waltham, USA
Labcycler	Sensoquest, Göttingen, Germany
Mr. Frosty™ Gefrierbehälter	Thermo Fischer Scientific, Waltham, USA
Merck's Muse Cell Analyzer	Merck KGaA, Darmstadt, Germany
Nanodrop 2000/c	Thermo, Fisher Scientific GmbH, Germany
Plate reader, TECAN 200M pro	TECAN, maennedorf, Switzerland
Primovert Microscope	CARL ZEISS, Oberochen, Germany
Privileg 8018e microwave	Privileg, Stuttgart, Germany
QIAxcel	QIAGEN, Venlo, Netherlands
Speed Vacuum concentrator	Thermo, Fisher Scientific GmbH, Germany
Trans-Blot Turbo	Bio-Rad, Hercules, USA

Equipment	Suppliers
Tubes vortex, schuett labortechnik	LABO
WTC binder Cell lines incubator,	Binder
ZOE fluorescent cell imager	Bio-Rad, Hercules, USA

2.1.2 Antibodies

Table 2: Summary of antibodies

Antibody	Technique	Dilution	Company
EZH2 (5246)	WB	1 : 1000	Cell Signaling, Germany
EZH2 (NCL-L-EZH2)	IHC	1 : 50	Leica, Germany
GADPH (5174)	WB	1 : 1000	Sigma-Aldrich, USA
H3k27me3 (39155)	WB	1 : 1000	ActiveMotif, USA
MTHFD2 (H00010797-M01)	WB	1 : 1000	Abnova, Germany
PARK7 (ab18257)	WB	1 : 1000	Abcam, UK

2.1.3 Cell lines

Table 3: List of cell lines

Cell line	KRAS status	Company
HCC44	c.G12C	American Type Culture Collection (ATCC)
H23	c.G12C	American Type Culture Collection (ATCC)
H1993	WT	American Type Culture Collection (ATCC)
HCC78	WT	American Type Culture Collection (ATCC)

2.1.4 siRNAs and guide RNAs

Table 4: List of siRNAs and guide RNAs (gRNA)

siRNA/gRNA	Company
All-Star Neg. Control siRNA (20 nmol) (1027281)	Qiagen GmbH, Hilden
Hs_EZH2 _6 siRNA (SI02633316)	Qiagen GmbH, Hilden

siRNA/gRNA		Company
Hs_EZH2 _7	siRNA (SI02665166)	Qiagen GmbH, Hilden
Hs_MTHFD2 _6	siRNA (SI02664921)	Qiagen GmbH, Hilden
Hs_MTHFD2_7	siRNA (SI02664928)	Qiagen GmbH, Hilden

2.1.5 Plasmids

Table 5: Summary of cell plasmids

Plasmids	Suppliers
$Kras^{G12C}$	OriGene Technologies, Inc. Maryland, USA (RG201222)
$Kras^{WT}$	Addgene, Watertown, MA, USA (75282)

2.1.6 Buffers and media

Table 6: List of buffers and media

Reagent	Composition
Ethanol (70 %)	700 ml Ethanol (99.9 %) in 1 L ddH2O
Blocking buffer	5 % milk powder in 1X TBS-T
Freezing medium	5 % DMSO in FCS
LB- Agar	15 g/L Agar-Agar in LB medium
LB medium	25 g LB medium in 1 L dH2O
Loading buffer (1 : 1/3)	500/250 µl 2x/4x Laemmli Sample Buffer, 500/750 µl 2-Mercaptoethanol
NP40 Lysis buffer	50 mM Tris/HCl (pH 7.6), 150 mM NaCl, 5 mM NaF, 1 % NP40
PBS	9.55 g/L PBS Dulbecco in ddH2O
Ponceau	0.5 g Ponceau, 5 ml 100 % glacial acetic acid in 500 ml with ddH2O
RPMI-1640	10 % FCS, 1 % Penstrip & 1 % glutamine
TBE buffer	100 ml 10X TBE buffer in 1 L ddH2O

Reagent	Composition
TBS	4.24 g Tris, 292.7 g NaCl, 26 g Tris-HCl solved in 1 L ddH2O
TBS-T	1 L 10X TBS, 9 L ddH2O and 10 ml Tween-20
Western blotting running buffer	100 ml 10X Tris/Glycine/SDS Buffer in 1 L ddH2O

2.1.7 Reagents and kits

Table 7: Summary of reagents and kits

Reagent	Supplier
10x Tris-Glycine-SDS Buffer	Bio-Rad, Feldkirchen, Germany
2x Laemmli Sample Buffer	Bio-Rad, Feldkirchen, Germany
4x Laemmli Sample Buffer	Bio-Rad, Feldkirchen, Germany
6x loading Dye	Thermo Fischer Scientific, Waltham, USA
Agar-Agar	Carl Roth GmbH & Co. KG, Karlsruhe
Ambion® DEPC-treated water	Invitrogen, Massachusetts, USA
Ampicillin	Gibco, Massachusetts, USA
BigDye XTerminator™ Purification Kit	Applied Biosystems, Massachusetts, USA
BigDye™ Terminator v1.1 Cycle Sequencing Kit,	Applied Biosystems, Massachusetts, USA
Celltiter 96 Aqueous one solution	Thermo, Fisher Scientific GmbH, Germany
CellTiter-Glo assay	Promega, Madison, WI, USA
DAB Substrate Kit	Agilent Technologies, California, USA
DC™ Protein Assay	Bio-Rad, Feldkirchen, Germany
Dh5alpha competent E. coli	Thermo, Fisher Scientific GmbH, Germany
DMEM medium	Gibco, Massachusetts, USA

Reagent	Supplier
DTT (10 mM)	Thermo, Fisher Scientific GmbH, Germany
EDTA	Merck, Darmstadt, Germany
EnVision Flex Target Retrieval Solution, pH high or low	Agilent Technologies, California, USA
Ethanol (99.9 %)	Merck, Darmstadt, Germany
ExoSAP-IT Express PCR Cleanup Reagents	Thermo Fischer Scientific, Waltham, USA
Fetal bovine serum (FbS)	Gibco, Massachusetts, USA
Glutamine	Gibco, Massachusetts, USA
Hipercfect	QIAGEN, Venlo, Netherlands
InnuPREP FFPE DNA Extraction Kit	Analytik Jena, Jena, Germany
Lauryl-β-D-maltoside	Merck, Darmstadt, Germany
LB medium	Carl Roth GmbH & Co. KG, Karlsruhe
Milk powder	Carl Roth GmbH & Co. KG, Karlsruhe
Mini-PROTEAN, Precast Gels	Bio-Rad, Feldkirchen, Germany
Na-pyruvate solution, 11360070	Gibco, Massachusetts, USA
Nitrocellulose membranes (Trans-Blot Bio-Rad Laboratories	Bio-Rad, Hercules, USA
P3000 reagent	Invitrogen, Massachusetts, USA
Pemetrexed	Hexal AG, Holzkirchen,Germany
PageRuler, Prestained 10 to 250 kDa	Thermo Fischer Scientific, Waltham, USA
Penicillin/Streptomycin (10,000 U/ml)	Gibco, Massachusetts, USA
Penicillin/Streptomycin, 15140163	Gibco, Massachusetts, USA
Phosphate buffered saline (PBS) Dulbecco	Merck, Darmstadt, Germany
Pierce™ BCA Protein Assay Kit	Thermo Fischer Scientific, Waltham, USA

Reagent	Supplier
Purgene® Core Kit A	QIAGEN, Venlo, Netherlands
QIAquick PCR Purification Kit	QIAGEN, Venlo, Netherlands
Reblot Plus Strong antibody stripping solution	Merck, Darmstadt, Germany
Rnase inhibitor 20 U/µl	Thermo Fischer Scientific, Waltham, USA
RPMI-1640 medium	Gibco, Massachusetts, USA
Taq DNA polymerase	New England Biolabs GmbH, Frankfurt am Main, Germany
Western Plus-ECL	PerkinElmer, USA
X-tremeGENE™ HP DNA Transfection Reagent	Sigma-Aldrich, St. Louis, Missouri, USA

2.1.8 Inhibitors

Table 8: Summary of inhibitors

Inhibitor	Supplier
AMG510 #HY-114277	MedChemExpress, Monmouth Junction, NJ, USA
GSK126 #S7061	Selleckchem, Houston, TX, USA,
DS18561882 #HY-130251	MedChemExpress, Monmouth Junction, NJ, USA

2.1.9 Disposals

Table 9: Summary of disposals

Disposal	Supplier
10 ml and 50 ml tubes	Cellstar, greiner bio-one, Germany
10 µl, 10 µl & 1000 µl filter/tips	SARSTEDT, Nümbrecht, Germany
10 cm culture dishes	Cellstar, greiner bio-one, Germany
12-well plates	Cellstar, greiner bio-one, Germany
1 ml, 5 ml, 10 ml & 25 ml pipettes	SARSTEDT, Nümbrecht, Germany

Disposal	Supplier
24-well plates	Cellstar, greiner bio-one, Germany
6-well plates	Cellstar, greiner bio-one, Germany
96-well plates	Cellstar, greiner bio-one, Germany
Cells scraper 25 cm	SARSTEDT, Nümbrecht, Germany
Cryopure	SARSTEDT, Nümbrecht, Germany
Disposable syringe, 10 ml	SARSTEDT, Nümbrecht, Germany
Disposable syringe, 2 ml Luer	SARSTEDT, Nümbrecht, Germany
DNA LoBind Tubes	Eppendorf, Hamburg, Germany
Muse® Count & Viability Assay kit	Merck, Darmstadt, Germany
QIAGEN Plasmid Midi Kit	QIAGEN, Venlo, Netherlands
QIAprep Spin Miniprep Kit	QIAGEN, Venlo, Netherlands
T175 culture flasks	SARSTEDT, Nümbrecht, Germany
T25 culture flasks	SARSTEDT, Nümbrecht, Germany
T75 culture flasks	SARSTEDT, Nümbrecht, Germany
Tissue embedding plastic cassettes	Merck, Darmstadt, Germany
Trans-Blot® Turbo™ RTA Mini Nitrocellulose Transfer Kit	Bio-Rad, Feldkirchen, Germany
Tube 30 ml, 84 x 30 mm, PP	SARSTEDT, Nümbrecht, Germany
Tube 7 ml, 50 x 16 mm, PS	SARSTEDT, Nümbrecht, Germany
1.5 and 2 ml microtubes	SARSTEDT, Nümbrecht, Germany
Microfilters, 0.2 µM, 0.45 µM	SARSTEDT, Nümbrecht, Germany

2.1.10 Chemical reagents

Table 10: Summary of chemicals

Reagent	Supplier
2-Mercaptoethanol	Carl Roth GmbH & Co. KG, Karlsruhe

Reagent	Supplier
Bovine Serum Albumin (BSA)	Carl Roth GmbH & Co. KG, Karlsruhe
EDTA-disodium salt	Carl Roth GmbH & Co. KG, Karlsruhe
Ethidium bromide	Carl Roth GmbH & Co. KG, Karlsruhe
G418 (Geneticin)	InvivoGen, California, USA
Glacial acetic acid	Merck, Darmstadt, Germany
HEPES	Sigma-Aldrich Co., St. Louis, USA
Isopropanol (100 %)	Merck, Darmstadt, Germany
Kanamycin	Gibco, Massachusetts, USA
$Na_4P_2O_7$	Carl Roth GmbH & Co. KG, Karlsruhe
NaCl	Carl Roth GmbH & Co. KG, Karlsruhe
Na-deoxycholate	Carl Roth GmbH & Co. KG, Karlsruhe
Naorthovandate	Sigma-Aldrich Co., St. Louis, USA
Na-orthovandate	Carl Roth GmbH & Co. KG, Karlsruhe
N-ethylmaleimide	Carl Roth GmbH & Co. KG, Karlsruhe
NP40	Carl Roth GmbH & Co. KG, Karlsruhe
Ponceau S	AppliChem GmbH, Darmstadt, Germany
Roche complete protease inhibitor cocktail (cOmplete™)	Merck, Darmstadt, Germany
Sodium Chloride (NaCl)	Carl Roth GmbH & Co. KG, Karlsruhe
Sodium dodecyl sulfate (SDS)	Carl Roth GmbH & Co. KG, Karlsruhe
Sodium fluoride (NaF)	Carl Roth GmbH & Co. KG, Karlsruhe
Sodium pyrophosphate tetrabasic decahydrate	Carl Roth GmbH & Co. KG, Karlsruhe
ß-glycerophosphate	Carl Roth GmbH & Co. KG, Karlsruhe
TRIS	Carl Roth GmbH & Co. KG, Karlsruhe
TRIS-hydrochloride	Carl Roth GmbH & Co. KG, Karlsruhe

Reagent	Supplier
Tween®20	AppliChem GmbH, Darmstadt, Germany
Urea	Sigma-Aldrich Co., St. Louis, USA
β-Glycerophosphate disodium salt hydrate	Carl Roth GmbH & Co. KG, Karlsruhe

2.1.11 Software

Table 11: List of software

Software/database	Supplier
3500 data collection software 3	Applied Biosystems, Massachusetts,USA
Endnote X9	Clarivate analytics, Philadelphia, USA
Graphpad Prism 8	GraphPad Software, La Jolla California USA (www.graphpad.com)
Geneious 11.0.4	Biomatters Ltd., Aukland, Neuseeland
Image J Version 1.52j	National Institutes of Health and the Laboratory, Bethesda, USA
i-contol™	Tecan Trading AG, Männedorf, Schweiz
Magellan™	Tecan Trading AG, Männedorf, Schweiz
Primer3Web	https://primer3.ut.ee
Microsoft Excel	Microsoft Corporation, Redmond, Washington, USA

2.2 Methods

2.2.1 Patients tissue samples

2.2.1.1 Tissue samples collection

In this study, all tissue samples were from NSCLC patients after surgical resections, which we obtained from the Department of Thoracic and Cardiovascular Surgery, University Medical Center Göttingen (UMG). Tissues were fixed with 4 % buffered formaldehyde, then embedded in paraffin (FFPE) for diagnosis. The experiments were approved by the ethics committee of the University Medical Center Göttingen (#1-2-08, 24-4-20) before they were performed. All patients included in this study gave informed consent. All procedures were performed according to the seventh version of the Declaration of Helsinki (World Medical Association 2013).

2.2.1.2 Immunohistochemistry (IHC)

Tissue samples were assembled in tissue microarrays (TMA) and EZH2 was immunohistochemically stained as published previously (Bohnenberger et al. 2018; Bremer et al. 2021). In Brief, 2 µm paraffin sections were incubated in EnVision Flex Target Retrieval Solution at high pH for EZH2 staining (PH = 9) (Dako, Japan) followed by incubation with a primary antibody against EZH2 (Leica, Germany, NCL-L-EZH2, 1 : 50) for 30 min at room temperature (RT). Primary antibodies were detected with HRP-conjugated secondary antibodies (EnVision Flex+, Dako). HRP was developed on DAB (Dako) substrate for 5 min. Mayer's hematoxylin staining was used for contrast. Sample staining was evaluated under light microscopy according to intensity, divided samples into three groups: zero = negative staining; one = weak staining intensity; two = strong staining intensity.

2.2.2 Cell culture

In this study, the human cell lines HCC44, H23, H1993, and HCC78 were cultured in RPMI 1640 growth media, containing 10 % fetal bovine serum (FBS), 1 % glutamine and 1 % Penicillin/Streptomycin. Cells were incubated in a humidified atmosphere of 5 % CO_2 at 37 °C. Cells were kept between 10 % and 80 % confluency and were passaged in a 1 : 4 dilution every three to four days.

For passaging or cryopreservation, cells were washed with PBS, detached with 0.05 % Trypsin-EDTA, centrifuged at 1200 rotations per minute (RPM) and either diluted in new flasks or resuspended in freezing media: 5 % dimethyl sulfoxide (DMSO) in Fetal calf serum

(FCS). For freezing, cells were aliquoted in cryovials and kept in a freezing container (Mr. Frosty) at -80 °C for 24 h. Cells were stored in liquid nitrogen for long periods or at -80 °C for short terms.

2.2.3 Protein preparation and Western blot

Whole-cell lysates were created by washing cells twice with cold PBS and subsequent centrifugation at 1400 RPM. Then cells were lysed for 30 min with NP40 lysis buffer on ice, centrifuged at 14000 g for 30 min, and the supernatant was collected. DC protein assay kit and plate reader (TECAN 200M pro) were used to determine the concentrations of the lysates. All the lysates were denatured with SDS loading buffer for 5 min at 95 °C. Equal amounts of lysates (e. g. 15 µg) were loaded on mini-protean precast gels (4 - 20 %). Proteins were separated at 80 V for 30 min followed by 120 V for 1 h 50 min. Proteins were blotted onto a nitrocellulose membrane for 7 min using the Trans-Blot Turbo system (Biorad). Successful blotting, protein separation, and initial loading were evaluated by Ponceau red solution. The Ponceau red was washed off with 1 x TBST buffer and membranes were blocked at RT with 5 % milk-TBST buffer for 1 h before incubation with primary antibodies overnight at 4 °C. Next day, membranes were washed using 1 x TBST buffer three times for 10 min. Then, membranes were incubated with the appropriate secondary antibody for 1 h at RT. Signals were developed using Fusion Fx, peQlab camera, and Western Plus-ECL. Signal bands and control intensity were measured by the software ImageJ and then normalized the sample signal intensity with loading controls.

2.2.4 Cell counting using Guava® Muse® cell analyzer

Cells were detached using 0.05 % EDTA-trypsin and stopped with cell culture medium as described. Cells were centrifuged at 1200 RPM for 5 min. Next, cells were resuspended with growth medium and 20 µl of cell suspension and 380 µl of counting/viability reagent were mixed in sample tubes. Samples were measured with MuseTM Cell Analyzer using the Count/Viability program.

2.2.5 MTS assay

MTS© was performed to quantify cell viability. The reduction of the MTS tetrazolium compound occurs in living cells via the NADPH dehydrogenase enzyme, which can only be reduced to the soluble formazan with a specific blue color by viable cells. The absorbance can be detected at 490 ~ 500 nm on a plate reader (Aslantürk 2018). In this assay, cells were incubated with an inhibitor or a DMSO control for indicated time periods after being seeded

in an appropriate density in 100 µl cell culture medium in 96-well plates. 20 µl of MTS reagent (Cell titer aqueous one solution, Promega) was added to each well, followed by incubation at 37 °C for 1 - 2 h. The TECAN 200m Pro plate reader was employed to measure the intensity of formazan dye with a wavelength of 660 nm. Treatment effects were calculated by comparison to DMSO controls. The half maximal inhibitory concentration (IC50) was determined by different drug concentrations inhibiting cell viability assuming a linear relation. Each assay was performed at least in triplicates and three independent experiments. Inhibitors used for this study are listed in Table 8.

2.2.6 ATP assay using CellTiter-Glo assay

The ATP luminescence assay was performed using the CellTiter-Glo assay (Promega, Madison, WI, USA), following the manufacturer´s instructions. Briefly, for individual experiments, cells were seeded in 96-well plates in 100 µl per well 24 h before treatment. After indicated time points, plates with specific treatments and controls were equilibrated to RT for 30 min and subsequently incubated with 100 µl CellTiter-Glo solution. After shaking (400 - 600 RPM) for 2 min to induce cell lysis, the plate was incubated at room temperature for 10 min to stabilize the luminescent signal. Next, luminescence was measured with a Tecan Reader Infinite 2000 (Tecan, Switzerland). Each assay was triplicated and experimented with three repetitions. Inhibitors used for this study are listed in Table 8.

2.2.7 Cell transfection using siRNA

For gene specific small interfering RNA (siRNA) knockdown lung cancer cell lines were inversely transfected with a concentration of 30 nM to 80 nM siRNA using HiPerFect Transfection Reagent (Qiagen). Allstar-negative siRNA was used as a scrambled control (Qiagen). Briefly, transfection medium containing 4 to 9.6 siRNA (20 µM) and 12 µl HiPerFect was supplemented to 100 µl with RPMI without FCS and incubated at RT for 20 min. Then it was dropwise added to 3 x 10^5 freshly seeded cells in a 2.3 ml culture medium. Cells were incubated for 48 h and then collected for protein isolation. A summary of siRNAs used is shown in Table 4.

2.2.8 Expression vector transfection and G418 selection

To determine the lowest lethal concentration of neomycin (G418), an antibiotic killing curve for the cell line was established. Generally, the pCMV6-Entry-KRAS^{G12C} vector (Origene Technologies Inc) can successfully be transfected to cell lines due to a neomycin resistance gene on the transfected plasmid. H1993 cells were incubated with high concentrations of

neomycin (G418) to perform antibiotic selection with a range from 100 μg/ml to 2000 μg/ml in normal growth medium for at least seven days. The lowest concentration of neomycin (G418) leading to the complete death of H1993 cells was 800 μg/ml.

Next, Escherichia coli (E. coli) bacteria and 1 μl added plasmid were incubated on ice for 30 min and was heat shocked at 42 °C for 45 sec, incubated on ice, and transformed into an LB medium without antibiotic for several hours. The bacteria were either plated on LB medium plates or inoculated in LB medium. Plates, as well as LB medium, contained the correct amount of the appropriate antibiotic with ampicillin (100 μg/ml). The liquid bacterial culture was incubated at 37 °C overnight in a shaking incubator and agar plates were kept in a 37 °C incubator overnight. Clones were amplified in an LB growth medium containing ampicillin and then purified with a plasmid maxiprep kit from Qiagen according to the manufacturer's protocol. Two plasmids transfection was performed using XtremeGENE HP DNA transfection reagent (Merck, Darmstadt, Germany). Briefly, the 100 μl transfection mixture contains 4 μl transfection reagent, 2 μg expression vector DNA, and serum-free cell medium. After RT incubation for 15 min, the mixture was dripped into 6-well plates with 2 ml culture medium and 3×10^5 cells were seeded on. H1993 cells were transfected with either pCMV6-Entry-$KRAS^{G12C}$ vector (Origene Technologies Inc., Rockville, MD, USA) or pBabe-$KRAS^{WT}$ vector (Addgene, Watertown, MA, USA). Cells expressing $KRAS^{G12C}$ were selected with G418 (800 μg/ml) and those expressing $KRAS^{WT}$ were selected with Puromycin (2 μg/ml). The cells were cultured for at least ten days and KRAS protein levels were detected by Western blotting.

2.2.9 DNA Isolation and KRAS Exon 2 Profiling

DNA was isolated from 10 μM FFPE tissue sections with the InnuPREP FFPE DNA Extraction Kit (Analytik Jena, Jena, Germany), according to the manufacturer's protocol. In brief, manual microdissection was performed before extracting DNA from lung adenocarcinoma tissues. First, hematoxylin and eosin-stained slides were inspected under a microscope to identify areas with sufficient tumor cells. The same areas were then reidentified on unstained 10 μM dewaxed, rehydrated, and air-dried tissue sections and separated with cannulas. DNA isolation from paraffin-embedded tissue was performed with the InnuPREP FFPE DNA Extraction Kit. Quantification and purity assessment of total DNA was confirmed by applying the NanoDrop spectrophotometer (Nano2000 Drop Thermo scientific).

2.2.9.1 DNA sanger sequencing of KRAS exons 2

Based on the specificity of Sotarasib towards the G12C mutation in clinical applications, we focused on exon 2 of KRAS. Primer3Web (https://primer3.ut.ee) was used to design the primers and was visited on 11 December 2021. DNA sequencing included the following main steps: Primers that span specific genomic regions were selected ($KRAS^{G12C}$: Forward: GGCCTGCTGAAAATGAC and Reverse: TGTATCAAAGAATGGTCCTGCAC). 200 ng quantitative DNA was amplified by polymerase chain reaction (PCR) in a labcycler (Sensoquest, Göttingen, Germany) using 2 × MyTaqTM HS Mix (PCRBIOSYSTEMS, London, UK) with indicated KRAS primers. After purification of PCR products, Sanger sequencing was performed on a 3500 Genetic Analyzer (Applied Biosystems Inc., Waltham, MA, USA) by the Applied BiosystemsTM Sanger sequencing kit (Applied Biosystems Inc., USA). DNA sequencing results were compared with $KRAS^{WT}$ using Geneious 11.1.3 software to analyze (http://www.geneious.com) (Figure 3). The detail of PCR is shown in Table 12.

Table 12: Summary of sanger sequencing

PCR reaction mixture		
Reagents	**volume (µl)**	
MyTaq Mix, 2x	10	
Primer forward	1 (10 µM)	
Primer reverse	1 (10 µM)	
Sample template	1	
ddH_2O	7	
Total	20	
PCR cycling protocol		
	Temperature	**Time**
Initial denaturation	95 °C	1 min
45 Cycles		
Denaturation	95 °C	15 sec
Annealing	58 °C	15 sec
Elongation	72 °C	10 sec
Final elongation	72 °C	1 min

Continued table

Storage	8 °C	∞
PCR cleanup mixture		
Reagents	**volume (µl)**	
ExoSAP	2	
ddH_2O	2	
PCR Product	10	
PCR cleanup protocol		
	Temperature	**Time**
Initial denaturation	37 °C	30 sec
25 Cycles		
Step 1	37 °C	15 min
Step 2	80 °C	15 min
Store forever	8 °C	∞
Cycle sequencing mixture		
Reagents	**volume (µl)**	
5x Big Dye buffer	1,5	
5x Big Dye	1	
Sequencing primer	3.2 (10 µM)	
ExoSAP DNA	2	
ddH_2O	2,3	
Total	10	
Cycle sequencing protocol		
	Temperature	**Time**
Initial denaturation	96 °C	1 min
25 Cycles		
Denaturation	96 °C	15 sec
Elongation	58 °C	15 sec
Store forever	8 °C	∞

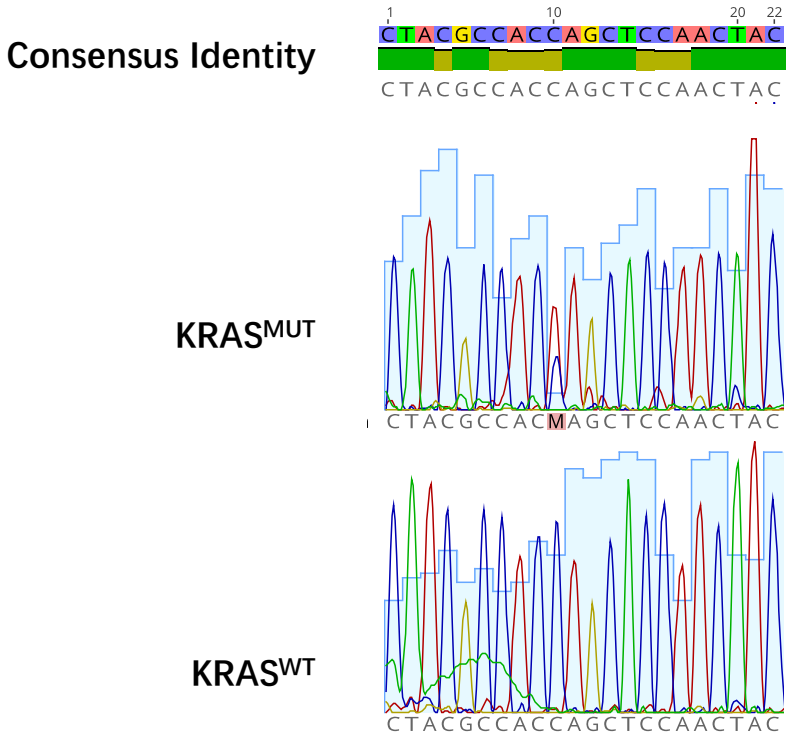

Figure 3: DNA sequencing of Exon 2 KRAS in AC patient samples $KRAS^{MUT}$ and $KRAS^{WT}$.

2.2.10 Statistical analysis

Statistical analysis was performed with GraphPad 8.0 (GraphPad Software LCC, San Diego, CA, USA). Two-group comparisons were performed with the Student's t-test. Correlations between KRAS gene mutation and EZH2 or MTHFD2 protein expression, or between EZH2 protein expression and MTHFD2 protein expression were performed by Chi-square test and Contingency test. Half-maximal inhibitory concentration (IC50) analysis was carried out using Pearson's correlation test. Comparisons of cell growth and drug resistance after treatment with different drug concentrations were performed by two-way ANOVA after log transformation and normalization.

The Kaplan-Meier method and the log-rank (Cox-Mantel) test were for survival analyses. The quantification of western blotting (WB) signal intensities was carried out by ImageJ (Schneider et al. 2012). Combination indexes (CI) were calculated based on the Chou-Talalay method. CompuSyn software was applied to calculate CI values, which identified the multiple drug synergistic effect. It can be classified into synergistic ($CI < 1$), additive ($CI = 1$) and antagonistic effects ($CI > 1$) (Chou, 2010). Biological triplicates were performed. The data depicted are the means ± SEMs. A p-value of < 0.05 was considered significant (* $p < 0.05$, ** $p < 0.01$, *** $p < 0.001$).

3 Results

3.1 EZH2 and MTHFD2 protein expression associated with KRAS Mutation Status and Clinicopathologic Characteristics in AC Patients

Aberrant KRAS activity has been connected to dysregulated metabolism and epigenetics in several cancer types (Han et al. 2022; Kerk et al. 2021; Riquelme et al. 2016). I first studied a cohort of 109 AC patients for activating KRAS mutations and MTHFD2 and EZH2 protein expression. Immunohistochemical staining (IHC) for MTHFD2 was obtained from Yao et al. (2021). All patients underwent surgical resection of the tumor without a history of chemotherapy. There were slightly more men (56 %) than women, and the median age at diagnosis was 67 years (range, 34 to 85). Most of the patients had moderately differentiated (G2) tumors, with the T1 - 2 stages accounting for 82.6 %, and most of them were node-negative (60.2 %). The median follow-up time was 23 months, and 48 % of patients died during follow-up. The patient's clinical characteristics are summarized in Table 13

Table 13: Clinical data summary. Modified from: (Li et al. 2022) (CC BY 4.0).

Histology	Pulmonary Adenocarcinoma
Total	109
Median age (range)	67 (34 - 85)
Gender, n (%)	
Female	48 (44.0)
Male	61 (56.0)
Degree of differentiation, n (%)	
I + II	78 (71.6)
III	31 (28.4)
T-stage, n (%)	
I + II	90 (82.6)
III + IV	19 (17.4)
Lymph node metastasis, n (%)	
No	62 (60.2)
Yes	41 (39.8)
pUICC, n (%)	
I + II	82 (75.2)
III + IV	27 (24.8)
Median survival time (months)	23

Histology	Pulmonary Adenocarcinoma
Reported deaths (%)	52 (47.7)

3.1.1 MTHFD2 Expression Correlate with KRAS Mutation Status

To investigate whether KRAS mutations are accompanied by MTHFD2 protein overexpression, we correlated the mutational status of exon 2 of the KRAS gene to MTHFD2 expression in AC.

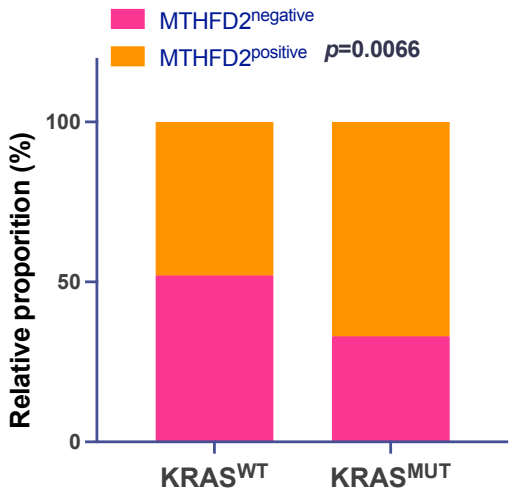

Figure 4: Correlation between MTHFD2 protein expression and KRAS gene mutation. MTHFD2 protein expression tested by IHC was compared to KRAS gene mutation tested by DNA sequencing in AC patient samples ($KRAS^{MUT}$: n = 18, $KRAS^{WT}$: n = 44). Modified from: (Li et al. 2022) (CC BY 4.0).

The correlation showed that in the $KRAS^{MUT}$ samples, 67 % were MTHFD2 positive, whereas 33 % were MTHFD2 negative. In the $KRAS^{WT}$ samples, 48 % were positive for MTHFD2 and 52 % were MTHFD2 negative. Chi-square test revealed a significant association between MTHFD2 high expressing and $KRAS^{MUT}$ tumors (p = 0.0066) (Figure 4).

Next, we tested whether the MTHFD2 protein expression level in $KRAS^{WT}$ and $KRAS^{MUT}$ AC samples had a prognostic relevance. Among 62 patients with clinical follow-up, eighteen samples were KRAS-mutated (G12C: n = 15, G12V: n = 3) and 44 were $KRAS^{WT}$. Kaplan-Meier curves and chi-square analysis showed a significant correlation between MTHFD2 and overall survival in $KRAS^{MUT}$ samples (p = 0.0178), but not in $KRAS^{WT}$ patients (p = 0.2906) (Figure 5).

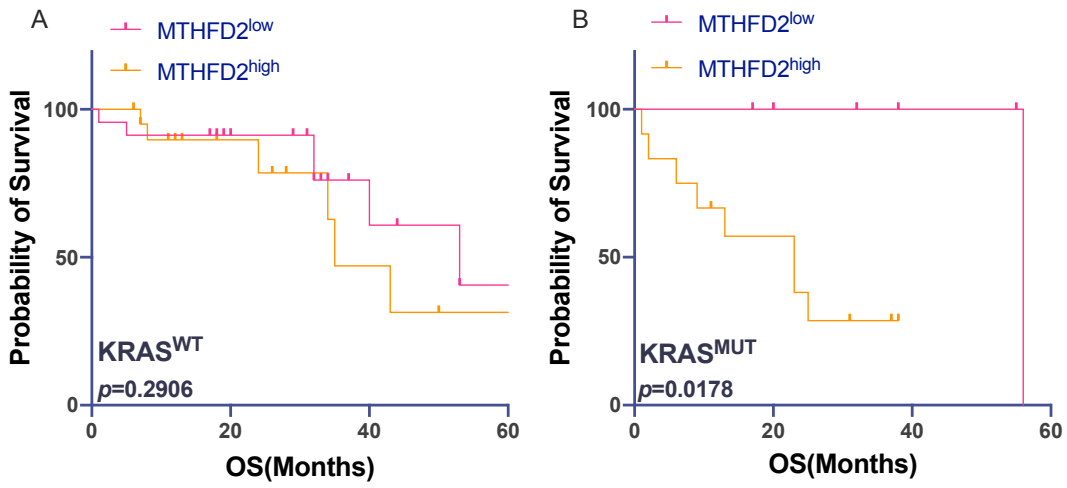

Figure 5: Survival analysis according to MTHFD2 protein expression in KRAS^{WT} and KRAS^{MUT} AC patients. Kaplan-Meier curves compared survival in low vs. high expression level of MTHFD2 in KRAS^{WT} (A) and KRAS^{MUT} (B) patient samples. P-values were calculated using Mantel-Cox Chi-square test. Modified from: (Li et al. 2022) (CC BY 4.0).

3.1.2 EZH2 protein expression in AC

109 AC patient samples were IHC stained for EZH2. The EZH2 protein expression was evaluated by a three-level scoring system: strong, weak, and negative expression (Figure 6).

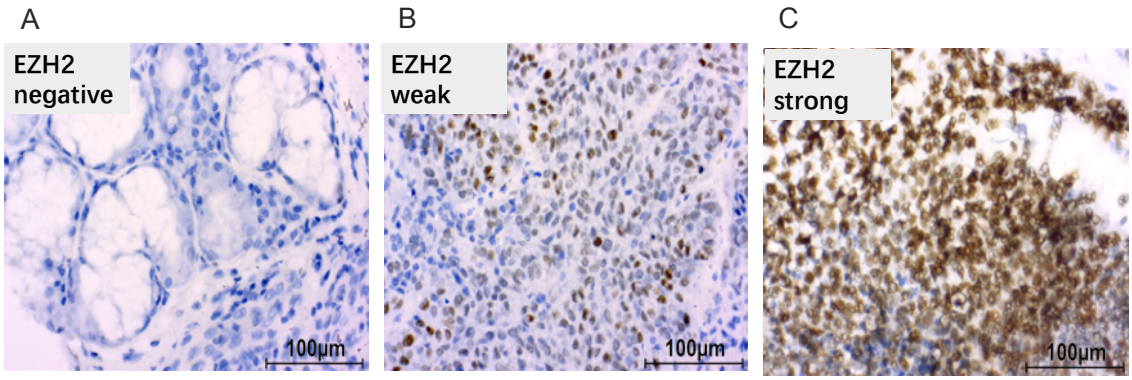

Figure 6: Immunohistochemically staining of EZH2 protein expression in AC patient tissue samples. Images show examples of EZH2 protein expression in negative (A), weak (B) and strong expressing samples (C). All images were captured at 40x magnification. Modified from: (Li et al. 2022) (CC BY 4.0).

From 109 evaluated AC samples EZH2 protein was strongly expressed in 38.5 %, the expression was found weak in 58.7 %, and was negative in 2.8 % (Figure 7A). Next, we investigated whether EZH2 protein expression had a prognostic relevance in AC. Kaplan-Meier curves alongside chi-square analysis showed a significantly better OS of patients with weak EZH2 expression (p = 0.0027) (Figure 7B).

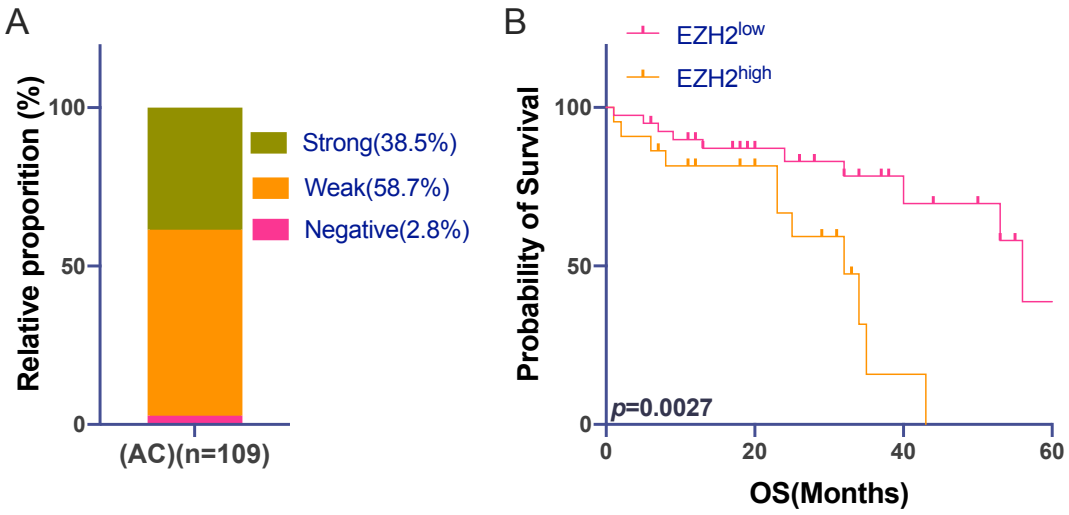

Figure 7: EZH2 protein expression in AC shows a prognostic relevance. (A) IHC detected the strength and prevalence of EZH2 protein expression in AC patients. (B) Kaplan-Meier analyses showed a significant association between EZH2 expression and survival in AC. Chi-square test was used for statistical analysis. Modified from: (Li et al. 2022) (CC BY 4.0).

3.1.3 Correlation between KRAS mutation and EZH2 protein expression in AC

The above-mentioned observation opened the question of whether KRAS mutations correlate with EZH2 protein overexpression. EZH2 expression was enriched in $KRAS^{MUT}$ cases with 50 % positive and 50 % negative samples.

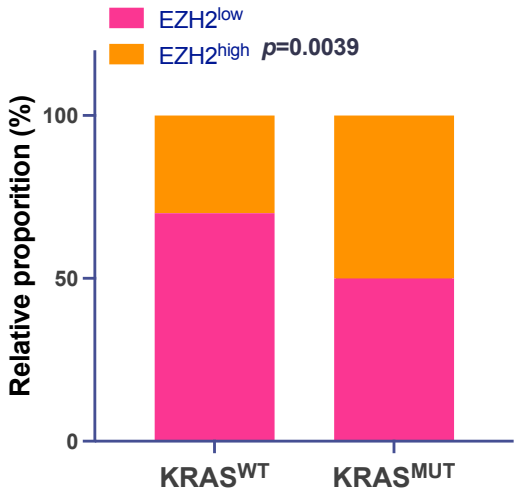

Figure 8: High EZH2 protein expression is enriched in cases with KRAS gene mutation. Correlation between EZH2 protein expression and KRAS gene mutation in AC samples. Chi-square test was used for statistical analysis. Modified from: (Li et al. 2022) (CC BY 4.0).

In the $KRAS^{WT}$ samples, only 30 % were positive for EZH2 expression, whereas 70 % were negative. Chi-square test showed a significant correlation between the high expression of EZH2 and $KRAS^{MUT}$ tumors ($p = 0.0039$) (Figure 8).

In addition, the expression of EZH2 and KRAS mutation was significantly associated with the occurrence of lymph node metastasis ($p = 0.0003$ and $p = 0.0052$, respectively) and a poor differentiation grade ($p < 0.0001$ and $p = 0.035$) as shown in Table 14.

Table 14: Correlation of EZH2 protein expression and KRAS gene mutation with clinicopathologic parameters. Modified from: (Li et al. 2022) (CC BY 4.0).

	IHC-EZH2	(n = 109)			KRAS (n = 62)			
Feature	**Cases**	**−**	**+**	**P-value**	**Cases**	**WT**	**MUT**	**P-value**
Gender, n (%)								
Female	48 (44)	33 (68.8)	15 (31.3)	0.0576	30 (48.4)	23 (76.7)	7 (23.3)	0.085
Male	61 (56)	34 (55.7)	27 (44.3)		32 (51.6)	21 (65.6)	11 (34.4)	
Age								
≥ 60	83 (76.1)	47 (56.6)	36 (43.4)	0.0026 **	46 (74.2)	35 (76.1)	11 (23.9)	0.0026 **
< 60	26 (23.9)	20 (76.9)	6 (23.1)		16 (25.8)	9 (56.3)	7 (43.7)	
Degree of differentiation, n (%)								
G1 - 2	78 (71.6)	54 (69.2)	24 (30.8)	< 0.0001 ***	47 (75.8)	35 (74.5)	12 (25.5)	0.035 *
G3	31 (28.4)	13 (41.9)	18 (58.1)		15 (24.2)	9 (60)	6 (40)	
T-stage, n (%)								
T1 - 2	90 (82.6)	55 (61.1)	35 (38.9)	0.7708	48 (77.4)	34 (70.8)	14 (29.2)	> 0.99
T3 - 4	19 (17.4)	12 (63.2)	7 (36.8)		14 (22.6)	10 (71.4)	4 (28.6)	
Lymph node metastasis, n (%)								
No	62 (60.2)	44 (71.0)	18 (29)	0.0003 ***	43 (69.4)	29 (67.4)	14 (32.5)	0.0052 **
Yes	41 (39.8)	19 (46.3)	22 (53.7)		19 (30.6)	16 (84.2)	3 (15.8)	
pUICC, n (%)								
I + II	82 (75.2)	52 (63.4)	30 (36.6)	0.3133	51 (82.3)	36 (70.6)	15 (29.4)	0.7528
III + IV	27 (24.8)	15 (55.6)	12 (44.4)		11 (17.7)	8 (72.7)	3 (27.2)	

(* $p < 0.01$, ** $p < 0.01$, *** $p < 0.001$)

To test the effect of EZH2 expression on tumor progression in dependence on KRAS mutation in AC we performed Kaplan-Meier curves alongside chi-square analysis. While in $KRAS^{WT}$ EZH2 expression levels did not significantly affect OS ($p = 0.1226$) (Figure 9A). However, in $KRAS^{MUT}$ cases, EZH2 expression significantly worsened patients' prognosis ($p = 0.0419$) (Figure 9B).

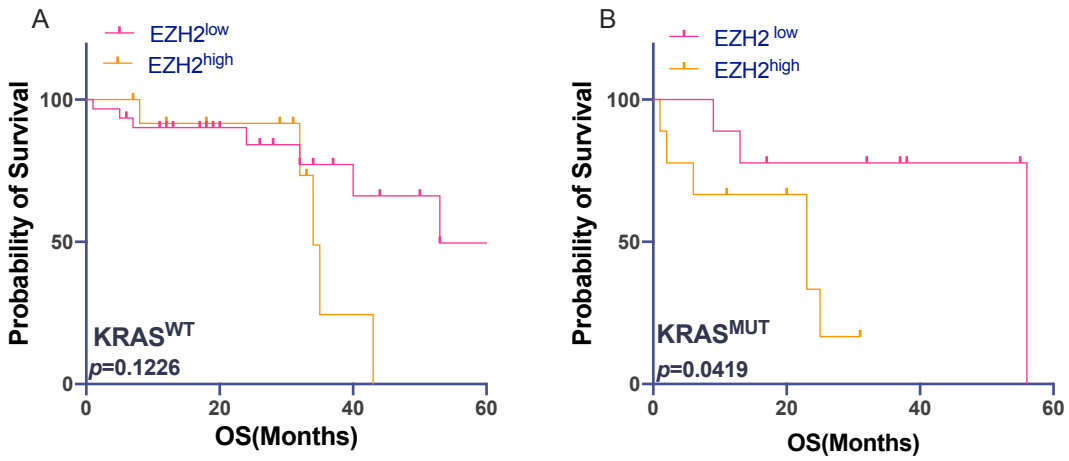

Figure 9: Survival analysis according to EZH2 protein expression with KRAS^{WT} and KRAS^{MUT} in AC patients. Kaplan-Meier curves compared survival in low vs. high expression levels of EZH2 in patient samples with KRAS^{WT} (A) and KRAS^{MUT} (B). P-values were calculated using Mantel-Cox Chi-square test. Modified from: (Li et al. 2022) (CC BY 4.0).

3.1.4 Correlating MTHFD2 protein expression with EZH2 and KRAS mutation

To further investigate the correlation between MTHFD2 or EZH2 protein expression and the KRAS mutational status, we evaluated MTHFD2 expression in either EZH2 low or EZH2 high expressing samples in dependence of KRAS mutation. This revealed a significantly increased MTHFD2 expression in EZH2 high expressing samples independent of KRAS mutations. This also revealed that MTHFD2 was significantly higher expressed in KRAS^{MUT} cases compared to WT in EZH2 high expressing tumors. Chi-square analysis showed a significant correlation ($p = 0.0005$) (Figure 10A). In addition, while MTHFD2 and EZH2 expression had no prognostic relevance in KRAS^{WT} cases ($p = 0.1152$) (Figure 10B), a combination of MTHFD2 and EZH2 low expression showed significantly better OS in KRAS^{MUT} patients ($p = 0.0128$) (Figure 10C).

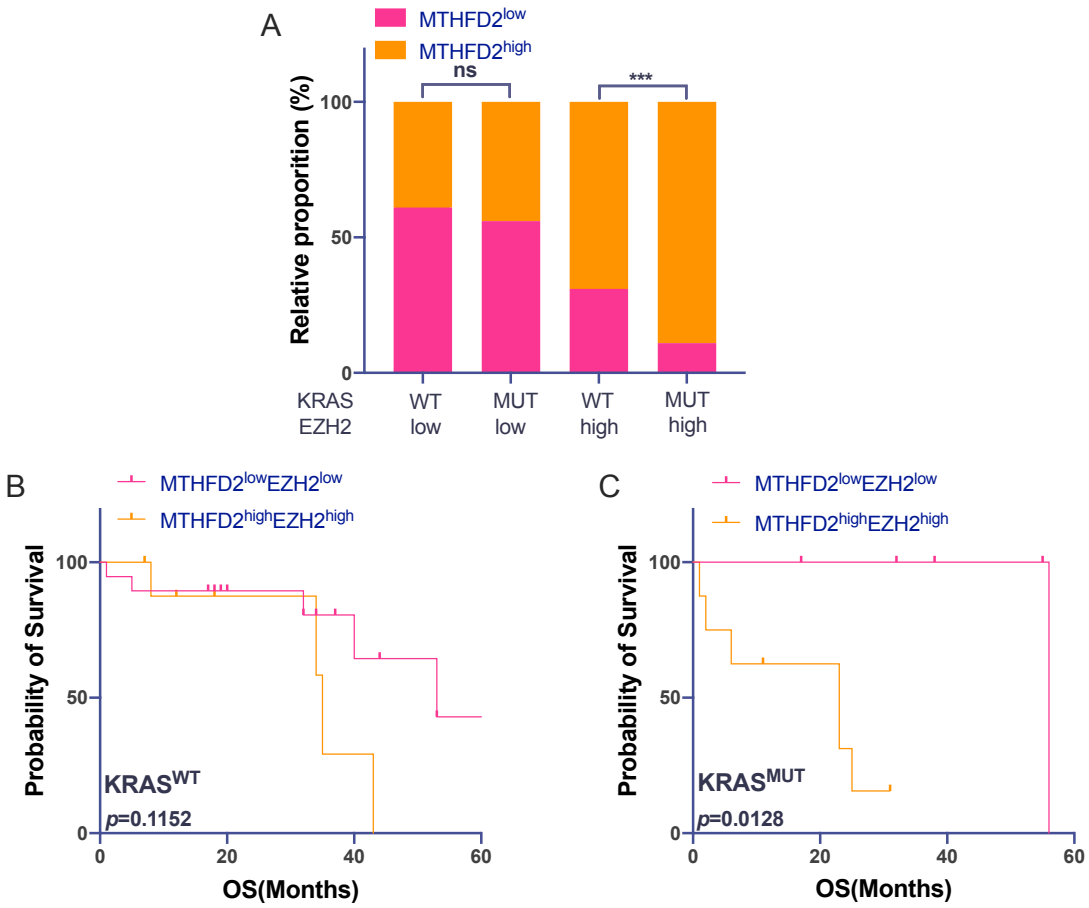

Figure 10: MTHFD2 protein expression and prognostic value is EZH2 and KRAS mutational status dependent. Correlation between EZH2 protein expression and KRAS mutation status in AC samples grouped according to EZH2 protein expression. Chi-square test was used for statistical analysis. Kaplan-Meier curves compared survival in low vs. high expression levels of both MTHFD2 and EZH2 in patient samples with $KRAS^{WT}$ (B) and $KRAS^{MUT}$ (C). P-values were calculated using Mantel-Cox Chi-square test (n = 62). Modified from: (Li et al. 2022) (CC BY 4.0).

3.2 MTHFD2 and EZH2 protein expression Depends on the Activity of Mutated KRAS in AC Cell Lines

To further investigate and validate the dependency of the MTHFD2 and EZH2 expression on aberrant KRAS activity in vitro we used two $KRAS^{G12C}$ (HCC44 and H23) and two $KRAS^{WT}$ (H1993 and HCC78) AC cell lines

3.2.1 MTHFD2 and EZH2 protein expression in AC cell lines

We initially tested the basic expression levels of MTHFD2 and EZH2 protein expression levels in the two $KRAS^{G12C}$ (HCC44 and H23) and two $KRAS^{WT}$ (H1993 and HCC78) AC cell lines by WB. Even though MTHFD2 and EZH2 protein was expressed in all four cell

lines (Figure 11A), quantitative analysis revealed up to 70 % higher levels of MTHFD2 and EZH2 in HCC44 and H23 in comparison to H1993 and HCC78 (Figure 11B, C).

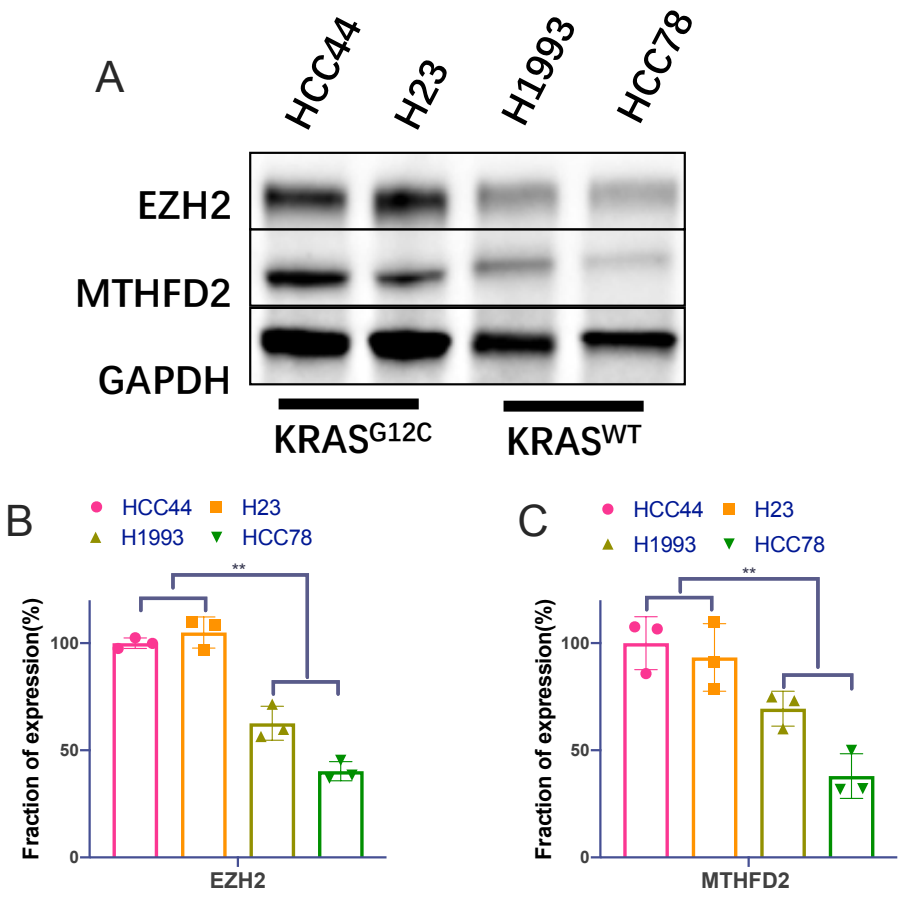

Figure 11: MTHFD2 and EZH2 expression depend on KRAS-mutated status in human AC cell lines. (A) WB analysis of EZH2 and MTHFD2 expression in the AC cell lines HCC44, H23, H1993, and HCC78. Quantification of EZH2 (B) and MTHFD2 (C) protein expression in the AC cell lines HCC44, H23, H1993, and HCC78. GAPDH was used as a loading control. Signal intensities of EZH2 and MTHFD2 from AC cell lines were normalized to GAPDH by ImageJ. Data presented as mean ± SEM. Representative of three independent experiments. (* $p < 0.05$, ** $p < 0.01$, *** $p < 0.001$, **** $p < 0.0001$). Modified from: (Li et al. 2022) (CC BY 4.0).

3.2.2 Establishing IC50 of Sotorasib (AMG510) in AC cell lines

To evaluate IC50 values of AMG510 (Sotorasib) in the 4 AC cell lines, we performed MTS with increasing concentrations (0 - 25 µM) for 72 h. Five biological replicates and three technical replicates were performed in the assay. MTS viability assay confirmed a good response of the $KRAS^{G12C}$ mutated HCC44 and H23 cell lines (IC50 < 9 µM), while H1993 and HCC78 did not respond and needed a more than four times higher concentration (IC50 > 40 µM) (Figure 12A).

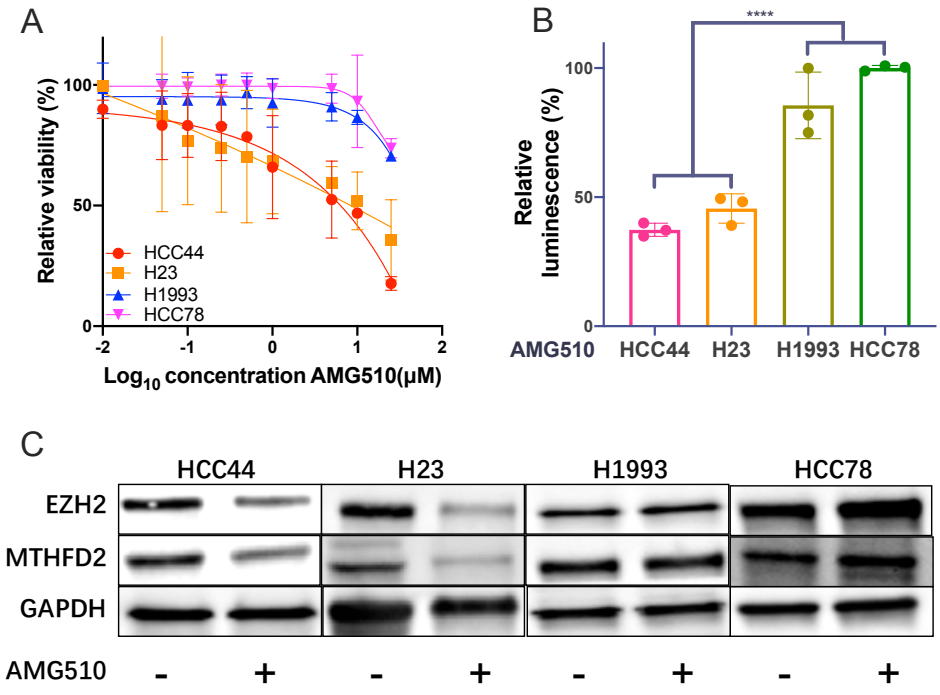

Figure 12: Effective to the KRAS^{G12C} inhibitor AMG510. (A) Inhibitory dose-response curves for AC cell lines treated with AMG510 were used in increasing concentrations for 72 h. The viability of the cells was measured using an MTS viability assay. (B) The cellular ATP level of HCC44, H23, H1993, and HCC78 cells after 48 h treatment with the KRAS^{G12C} inhibitor AMG510 (4 µM) were measured using the CellTiter-Glo assay. (C) EZH2 and MTHFD2 expression in AC cells after treatment with AMG510 (4 µM) for 48 h. GAPDH was used as a loading control. Signal intensities of EZH2 and MTHFD2 from AC cell lines were normalized to GAPDH by ImageJ. Data presented as mean ± SEM. Representative of three independent experiments. (* $p < 0.05$, ** $p < 0.01$, *** $p < 0.001$, **** $p < 0.0001$). Modified from: (Li et al. 2022) (CC BY 4.0).

A metabolic link to KRAS mutation was found by measuring ATP using the CellTiter-Glo assay after treatment with AMG510 (4 µM) for 48 h. This showed a significant decrease in cellular ATP levels only in the KRAS^{G12C} cell lines HCC44 and H23, whereas in H1993 and HCC78 no significant reduction in ATP was detected (Figure 12B). To investigate the influence of a KRAS aberration on MTHFD2 and EZH2 expression, we performed WB after 48 h treatment with 4 µM AMG510. Immunoblotting showed that EZH2 and MTHFD2 protein levels were significantly decreased only in KRAS^{G12C} cell lines HCC44 and H23, whereas there were no changes in KRAS^{WT} cell lines H1993 and HCC78 (Figure 12C).

3.2.3 Overexpression of KRAS^{G12C} in H1993 and HCC78 increases MTHFD2 and EZH2 expression

Since MTHFD2 and EZH2 were strongly expressed in KRAS^{G12C} cell lines, we wanted to know whether the G12C mutation of KRAS is responsible for the increased expression of

these two genes. We, therefore, overexpressed KRAS^{G12C} in H1993 and HCC78 with either the pCMV6-Entry- KRAS^{G12C} vector or a pBabe-KRAS^{WT} vector. WB against MTHFD2 and EZH2 confirmed the activation of KRAS in the KRAS^{WT} transfected cell line H1993 compared to either KRAS^{WT}-vector or control cells (without transfection) (Figure 13A). Quantification revealed that transient overexpression of KRAS^{G12C} in H1993 (KRAS^{G12Cvec}) raised the expression of MTHFD2 and EZH2 by about 30 % (Figure 13B, C).

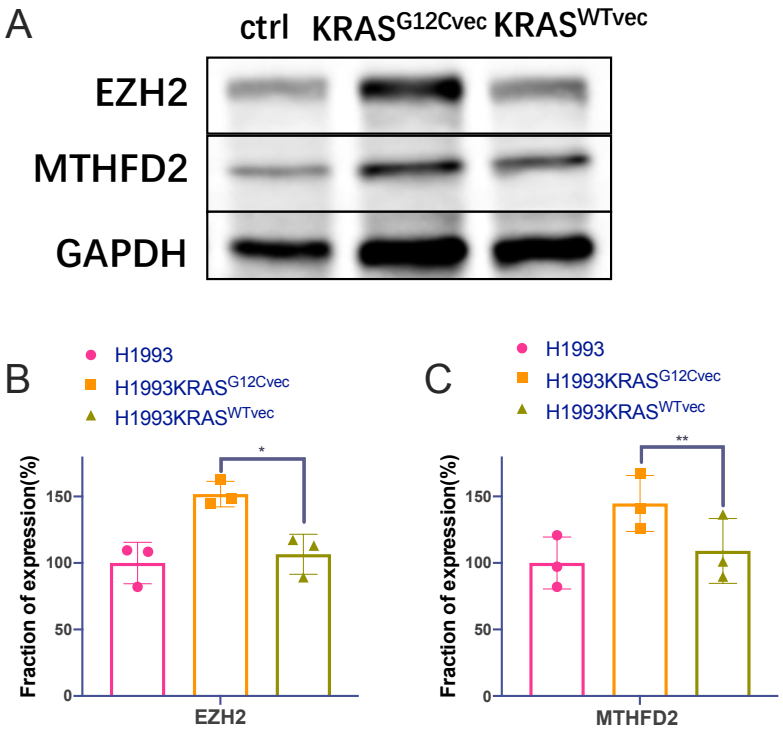

Figure 13: Increased EZH2 and MTHFD2 expression by constitutive expression of KRAS^{G12C} in H1993. (A) Western blot analysis of EZH2 and MTHFD2 expression in H1993 cells transfected with Kras^{G12Cvec} or Kras^{WTvec} plasmids. Quantification of EZH2 (B) and MTHFD2 (C) protein expression in H1993 expressing Kras^{G12Cvec} or Kras^{WTvec} or WT. Data presented as mean ± SEM. Representative of three independent experiments. (* $p < 0.05$, ** $p < 0.01$, *** $p < 0.001$, **** $p < 0.0001$). Modified from: (Li et al. 2022) (CC BY 4.0).

We then tested the response of KRAS^{G12C}-overexpressing H1993 cells in comparison to KRAS^{WT} cells towards sotorasib. After treatment with AMG510 (4 µM) for 48 h, the viability of KRAS^{G12C} transfected cell decreased by about 40 % (Figure 14A) and MTHFD2 and EZH2 protein expression was remarkably decreased in comparison to KRAS^{WT} control cells (Figure 14B).

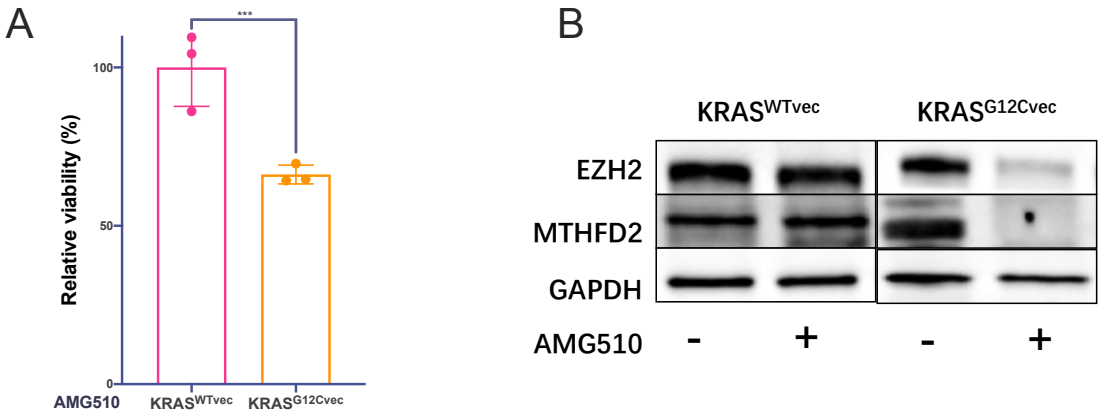

Figure 14: Cellular survival and protein levels of EZH2 and MTHFD2 in Kras^{WTvec}- or Kras^{G12Cvec}-transfected H1993 cells after treatment with AMG510. (A) Cell viability of control cells (Kras^{WTvec}) and KRAS^{G12C} overexpressing H1993 cells (KRAS^{G12Cvec}) after treatment with the KRAS^{G12C} inhibitor AMG510 (4 µM) for 48 h were measured using the CellTiter-Glo assay. Results are shown after normalization to DMSO control. (B) WB analysis of EZH2 and MTHFD2 proteins expression in Kras^{WTvec} and Kras^{G12Cvec} transfected H1993 cells after treatment with AMG510 (4 µM) or DMSO controls for 48 h. GAPDH was used as a loading control. Signal intensities of EZH2 and MTHFD2 from AC cell lines were normalized to GAPDH by ImageJ. Data presented as mean ± SEM. Representative of three independent experiments. (* $p < 0.05$, ** $p < 0.01$, *** $p < 0.001$, **** $p < 0.0001$). Modified from: (Li et al. 2022) (CC BY 4.0).

3.3 MTHFD2 expression is dependent on EZH2 in KRAS^{G12C} Cell Lines

3.3.1 EZH2 knock down leads to MTHFD2 reduction

To investigate the relationship between EZH2 and MTHFD2 and aberrant KRAS activity in AC cells, we used two specific siRNAs to knock down EZH2. WB results revealed a diminished expression of MTHFD2 only in KRAS^{G12C} after the reduction of EZH2 (Figure 15A, C). This was quantified for both siRNAs and showed an equal reduction of MTHFD2 and EZH2 in the KRAS^{G12C} cells HCC44 and H23, whereas no significantly decreased expression of MTHFD2 was found in KRAS^{WT} EZH2 knockdown cell lines H1993 and HCC78 (Figure 15B, D).

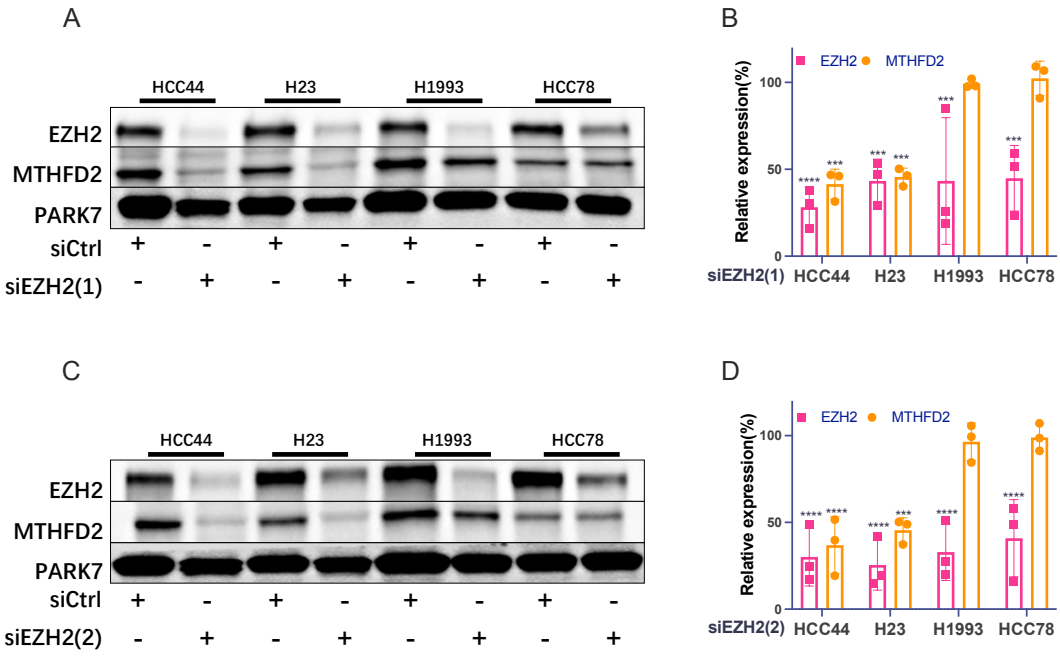

Figure 15: Knockdown of EZH2 significantly reduces MTHFD2 expression of the KRAS^{G12C} cell lines HCC44 and H23. (A and C) Western blot analysis of EZH2 and MTHFD2 in the four AC cell lines HCC44, H23, H1993, and HCC78 after EZH2 siRNA #1 and #2 knockdown, respectively. GAPDH was used as a loading control. Signal intensities of EZH2 and MTHFD2 from AC cell lines were normalized to GAPDH by ImageJ. (B and D) Related quantification of EZH2 and MTHFD2 protein expression after EZH2 siRNA #1 and #2 knockdown, respectively. Data presented as mean ± SEM. Representative of three independent experiments. (* $p < 0.05$, ** $p < 0.01$, *** $p < 0.001$, **** $p < 0.0001$). Modified from: (Li et al. 2022) (CC BY 4.0).

Then we were interested in whether EZH2 expression also depended on MTHFD2. Therefore, we targeted MTHFD2 with two specific siRNAs and tested the expression of EZH2 and MTHFD2 by WB (Figure 16A, C). In contrast to the EZH2 knockdown where MTHFD2 was co-regulated after MTHFD2 suppression neither AC cell line showed a reduction of EZH2 expression. Quantification of WB signals also showed no significant reduction of EZH2 after MTHFD2 siRNA treatment neither in the KRAS^{WT} nor in the KRAS^{G12C} cells (Figure 16B, D). These data strongly suggested that MTHFD2 expression is dependent on EZH2 in the KRAS^{G12C} AC cells.

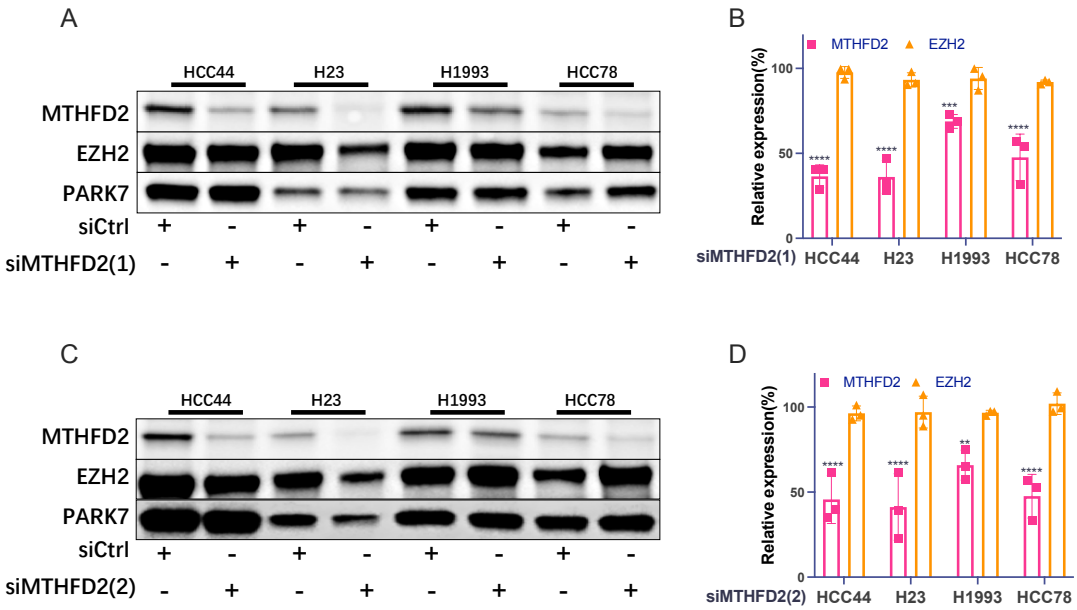

Figure 16: Knockdown of MTHFD2 does not influence EZH2 expression. (A and C) WB analysis of MTHFD2 and EZH2 in the four AC cell lines HCC44, H23, H1993, and HCC78 after MTHFD2 after knocking down with siRNA #1 and #2, respectively. GAPDH was used as a loading control. Signal intensities of EZH2 and MTHFD2 from AC cell lines were normalized to GAPDH by ImageJ. (B and D) Related quantification of MTHFD2 and EZH2 protein expression after MTHFD2 siRNA #1 and #2 knockdown, respectively. Data presented as mean ± SEM. Representative of three independent experiments. (* $p < 0.05$, ** $p < 0.01$, *** $p < 0.001$, **** $p < 0.0001$). Modified from: (Li et al. 2022) (CC BY 4.0).

3.3.2 Pharmacological inhibition of EZH2 or MTHFD2 shows a better response in KRAS^{G12C} AC cell lines

To elucidate the response of AC cell lines towards the pharmacological EZH2 inhibitor GSK126 and the MTHFD2 inhibitor DS18561882, we established the IC50 of the KRAS^{G12C} cell lines HCC44 and the KRAS^{WT} cell line H1993. For GSK126 the concentrations ranged from 0 to 15 µM and for DS18561882 from 0 to 100 µM. The concentration ranges were taken from studies using these inhibitors before (Kawai et al. 2019; Smith et al. 2019).

Interestingly, the IC50s of HCC44 were three to two times lower than in H1993 with an IC50 of GSK126 (4.89 µM) and IC50 of DS18561882 (23.259 µM) in HCC44 and an IC50 of GSK126 (13.26 µM) and IC50 of DS18561882 (45.49 µM) in H1993 (Figure 17).

To prove the effect of GSK126 on EZH2, we next investigated the methylation status of the H3K27. By immunoblotting, we tested the methylation of H3K27 (H3K27me3) and again EZH2 and MTHFD (Figure 18A). Without decreasing signals on EZH2 levels its inhibition was confirmed by a decreased tri-methylation of H3K27 in all four cell lines. Astonishingly, MTHFD2 levels were decreased upon GSK126 treatment only in the KRAS^{G12C} cell lines HCC44 and H23.

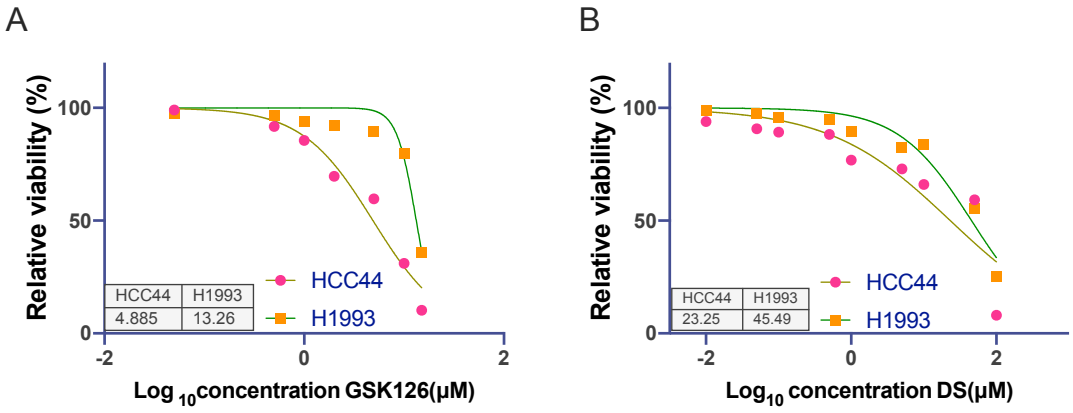

Figure 17: IC50 values and inhibitory curve in the AC cell lines HCC44 (KRAS^{G12C}) and H1993 (KRAS^{WT}). HCC44 and H1993 were treated with the EZH2 inhibitor GSK126 for 72 h. The EZH2 inhibitor GSK126 and the MTHFD2 inhibitor DS (DS18561882) were used in increasing concentrations. The viability of the cells was measured using an MTS viability assay. Data presented as mean ± SEM. Representative of three independent experiments. Modified from: (Li et al. 2022) (CC BY 4.0).

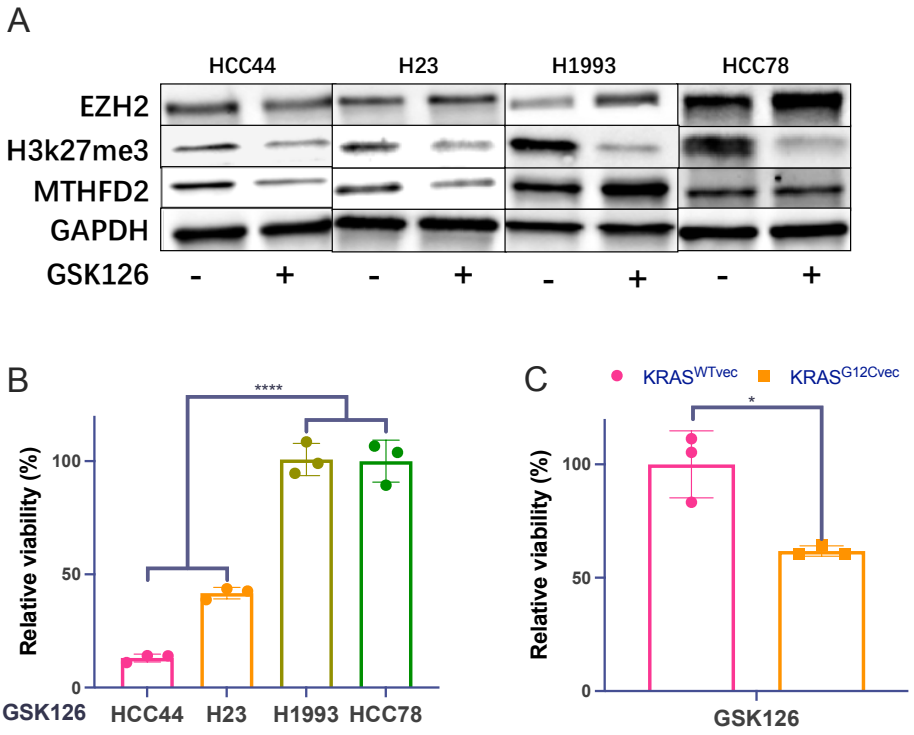

Figure 18: GSK126 treatment leads to a decreased H3K27 trimethylation in all cells and reduces MTHFD2 in KRAS^{G12C} AC cells. (A) Western blot analysis showing EZH2 and MTHFD2 expression in the four AC cell lines HCC44, H23, H1993, and HCC78 after 48 h treatment with the EZH2 inhibitor GSK126 (5 µM). GAPDH was used as a loading control. Representative of three independent experiments. (B) The cellular viability of the four described cell lines treated as in (A). (C) The cellular survival of KRAS^{WT}- and KRAS^{G12C}-transfected H1993 cells after 48 h treatment with GSK126 (5 µM). Data presented as mean ± SEM. Representative of three independent experiments. (* $p < 0.05$, ** $p < 0.01$, *** $p < 0.001$, **** $p < 0.0001$). Modified from: (Li et al. 2022) (CC BY 4.0).

This indicated an epigenetic and KRAS dependent regulation of MTHFD2 and 1CM. When we tested cellular viability after treatment with 5 µM GAK126 for 48 h, we only found HCC44 and H23 responding. H1993 and HCC78 did not show significantly different viability indicating that GSK126 indirectly acts on 1CM only in KRAS mutated cells (Figure 18B). We could also prove the dependency on KRAS activity by treating H1993 $KRAS^{G12Cvec}$ and vector controls with GSK126. The constitutive $KRAS^{G12C}$ expressing H1993 was responding similarly upon GSK126 treatment as HCC44 and H23 and compared to $KRAS^{WT}$ vector control (Figure 18C).

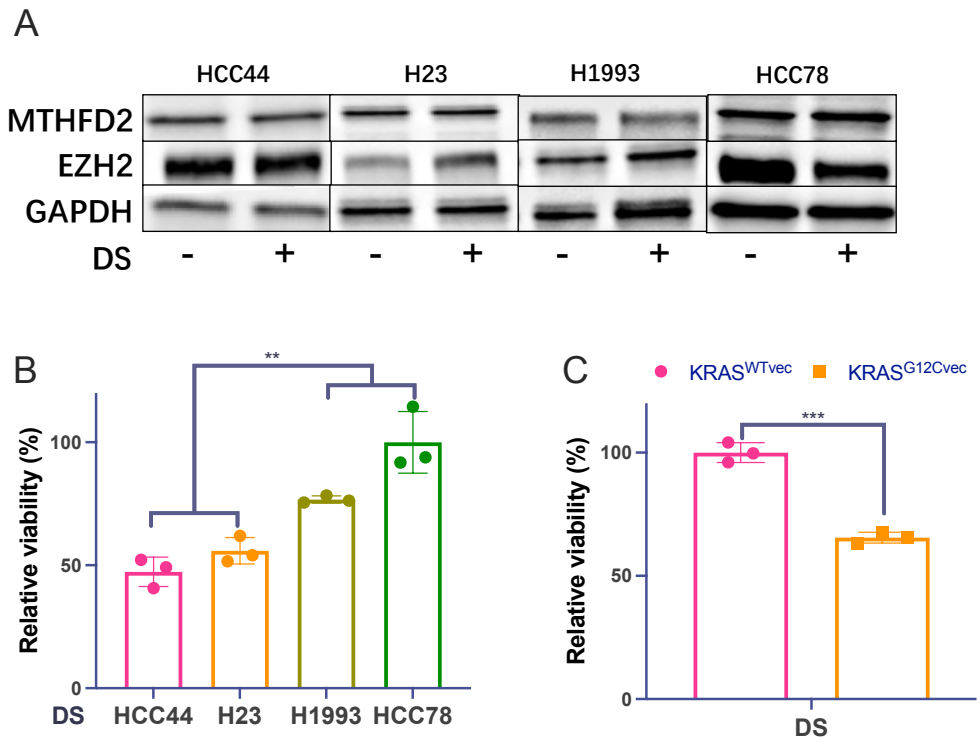

Figure 19: DS18561882 reduces cell viability in KRAS aberrant cells without affecting EZH2. (A) Western blot analysis showing EZH2 and MTHFD2 expression in the four AC cell lines HCC44, H23, H1993, and HCC78 after 48 h treatment with the MTHFD2 inhibitor DS (DS18561882) (20 µM). GAPDH was used as a loading control. (B) The cellular viability of the four described cell lines treated as in (A). (C) The cellular viability of $KRAS^{WTvec}$ and $KRAS^{G12Cvec}$ H1993 cells after 48 h treatment with DS18561882 (20 µM). Data presented as mean ± SEM. Representative of three independent experiments. (* $p < 0.05$, ** $p < 0.01$, *** $p < 0.001$, **** $p < 0.0001$). Modified from: (Li et al. 2022) (CC BY 4.0).

Similar observations were made with siRNA against MTHFD2. Treating AC cells with the specific MTHFD2 inhibitor DS18561882 showed no difference in EZH2 expression (Figure 19A). However, DS18561882 reduced cellular viability significantly stronger in the $KRAS^{G12C}$ HCC44 and H23 than in the KRAS cells (Figure 19B). Also, in the H1993 $KRAS^{G12Cvec}$ cells,

DS18561882 reduced cell viability similar to KRAS^{G12C} cells while KRAS^{WTvec} remained unaffected (Figure 19C).

3.4 Combinational Treatment with sotorasib, GSK126, and DS18561882

Our results showed that MTHFD2 and EHZ2 were strongly dependent on activating KRAS mutations, we decided to test whether a combined treatment may have a synergistic effect on KRAS^{MUT} cell viability. Therefore, we treated HCC44 with increasing concentrations of AMG510, GSK126, and DS18561882 in various combinations and compared them to single treatments. Response curves were compared, and significance values were calculated using two-way Anova. While single treatments of AMG510, GSK126, and DS18561882 showed similar responses, combinations of AMG510/DS18561882, AMG510/GSK126, and DS18561882/GSK126 showed significantly better effects. Interestingly, the combination of DS18561882 and GSK126 had the best response, independent of KRAS^{G12C} inhibition (Figure 20).

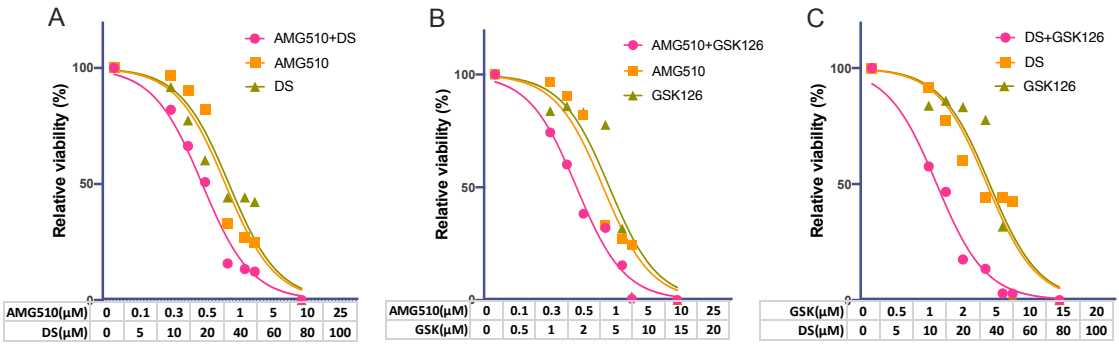

Figure 20: Synergistic effect of KRAS, EZH2, and MTHFD2 co-inhibition in the KRAS^{G12C} cell line HCC44. (A) Cellular viability of HCC44 after treatment with AMG510, DS (DS18561882), or the combinational treatment at described concentrations for 72 h. (B) Cellular viability of HCC44 after treatment with AMG510, GSK126, or the combinational treatment at described concentrations for 72 h. (C) Cellular survival of HCC44 after treatment with DS (DS18561882), GSK126, or the combinational treatment at described dosages for 72 h. The viability of the cells was measured using an MTS viability assay. Data presented as mean ± SEM. Representative of three independent experiments. Modified from: (Li et al. 2022) (CC BY 4.0).

To evaluate the synergy of the combinational treatment we generated a combination index value using the Chou-Talalay method (CompuSyn software). CI values: ($CI < 0.9$, $CI = 0.9 \sim 1.1$, and $CI > 1.1$) to indicate synergistic, additive, and antagonistic effects, respectively. All combinations showed an increased and synergistic reduction in cell survival

compared to single treatments. In particular, the combination of GSK126 and DS18561882 showed a remarkable response that was comparable to $KRAS^{G12C}$ inhibition at relatively low concentrations (Figure 21).

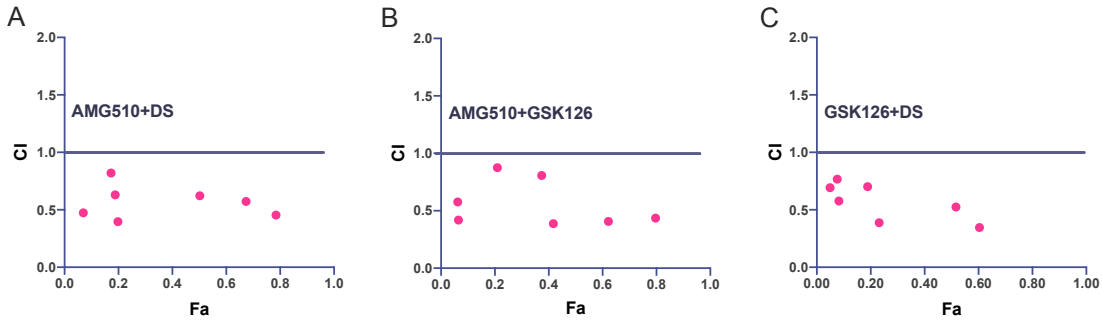

Figure 21: Combination index values indicated the type of interaction between KRAS, EZH2, and MTHFD2 inhibitors. The effect of combined inhibition was evaluated with an MTS viability assay after 72 h treatment. Combination index (CI) plot for AMG510, DS (DS18561882), and GSK126 in HCC44. CompuSyn was used by a computer to simulate CI values as a function of the fraction of cell viability inhibition; the actual experimental points are represented by pink dots. CI values: CI < 0.9 for synergism, CI = 0.9 ~ 1.1 for additive effect, and CI > 1.1 for antagonism. Modified from: (Li et al. 2022) (CC BY 4.0).

3.5 Combinational Treatment of $KRAS^{G12C}$ with Pemetrexed and Inhibitors

Studies have previously indicated that high MTHFD2 expression induced resistance against Pemetrexed (PTX) (Yao et al. 2021) and that the reduction of $KRAS^{G12C}$ increases response to PTX (Moran et al. 2014).

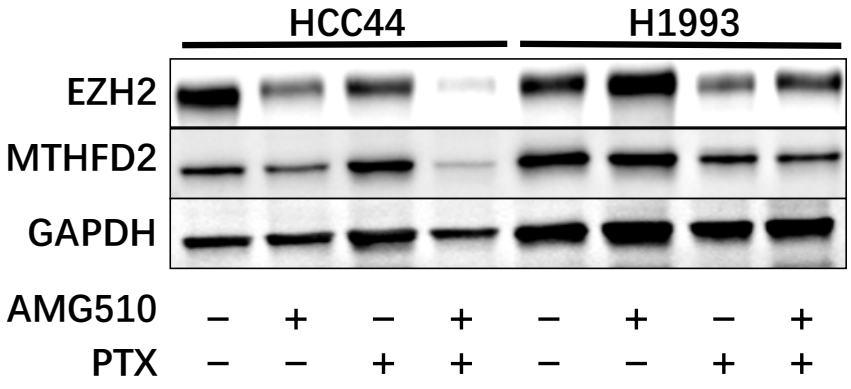

Figure 22: The effect of PTX alone and in combination with AMG510. Western blot analysis showing EZH2 and MTHFD2 expression of HCC44 and H1993 after 48 h single treatment with AMG510 (2 µM) or PTX (20 µM) or in combination. GAPDH was used as a loading control. Modified from: (Li et al. 2022) (CC BY 4.0).

To test whether the inhibition of KRAS^{G12C} restores the sensitivity of HCC44 cells to PTX, HCC44, and H1993 cells were incubated either with AMG510 (2 µM) or PTX (20 µM) and in combination. After a single treatment, EZH2 and MTHFD2 protein levels were only partially reduced. However, the combination of the two agents almost completely suppressed EZH2 and MTHFD2 expression in HCC44, whereas it was almost unaffected in H1993 (Figure 22).

To investigate whether PTX also acts synergistically with KRAS^{G12C} inhibitors or GSK126 and DS18561882, we combined treatments and evaluated IC50 values. We used increasing concentrations of PTX (0.005 - 50 µM) and single concentrations of GSK126 (2.5 µM), DS18561882 (10 µM), and AMG510 (2 µM) to treat HCC44 and H1993 over 72 h. The combination of PTX with DS18561882 or GSK126 showed about a 10-fold increase in response in comparison to PTX alone. Combining PTX with AMG510 (2 µM) had an 80-fold increased killing effect in the KRAS mutated HCC44 (Figure 23A). In contrast, in H1993 cells, no additional effect was observed (Figure 23B).

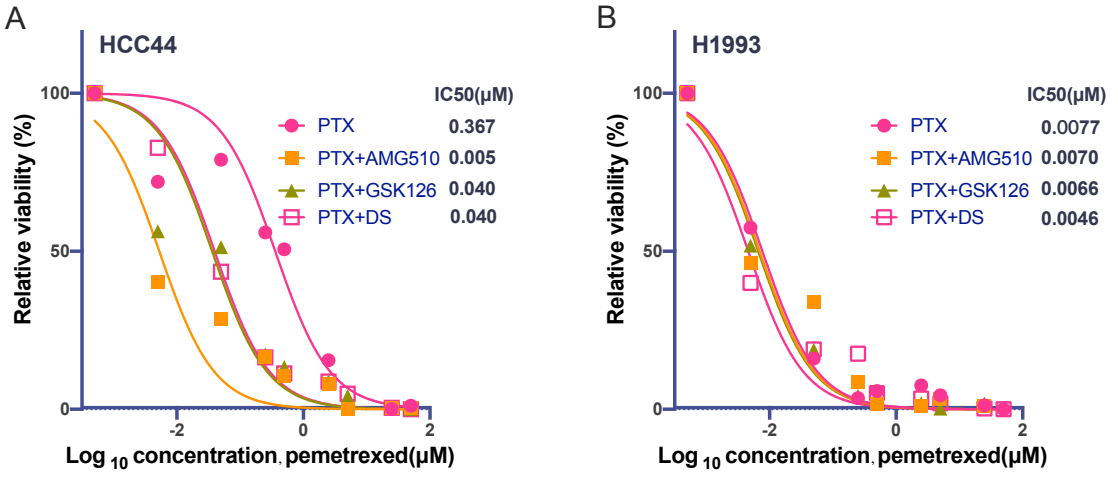

Figure 23: Combinational Treatment of PTX and 3 inhibitors in AC cell lines. Dose-response curve of HCC44 (A) and H1993 (B) after 72 h single treatment with PTX (0.005 – 50 µM) alone or in combination with AMG510 (2 µM), GSK126 (2.5 µM), or DS (DS18561882) (10 µM), respectively. The viability of the cells was measured using an MTS viability assay. Data presented as mean ± SEM. Representative of three independent experiments. Modified from: (Li et al. 2022) (CC BY 4.0).

4 Discussion

4.1 EZH2 and MTHFD2 Expression associated with KRAS Mutation Status in AC

The invention and FDA approval of Sotorasib and Adagrasib have considerably improved the clinical course of patients with $KRAS^{G12C}$ mutated AC. However, for about two-thirds of patients not responding or carrying different activating KRAS mutations there is still an urgent need for alternative therapeutic strategies. The involvement of aberrant KRAS in regulating 1CM and in DNA imprinting opens new opportunities for differential or combinatorial treatments.

KRAS mutations play a crucial role in the regulation of tumor metabolism (Stine et al. 2022; Yang et al. 2020; Ying et al. 2012) by increasing the need for energy, elevating aerobic glycolysis, and by promoting chemoresistance, tumor progression, and metastasis (Hanahan and Weinberg 2011; Kaelin and Thompson 2010; Tao et al. 2014; Zhou et al. 2012). Recent studies have shown that KRAS mutations increase the dependency of NSCLC and CRC on 1CM (Ju et al. 2019; Moran et al. 2014; Yao et al. 2021), They demonstrated that MTHFD2 is crucial for NSCLC cell lines and a prognostic factor in AC (Yao et al. 2021). High expression levels of MTHFD2 have been shown to correlate with tumor recurrence and a bad prognosis in many kinds of solid and hematologic malignancies. In AC, colorectal, and pancreatic cancer MTHFD2 has been associated with resistance against gemcitabine and pemetrexed (Bonagas et al. 2022; Ju et al. 2019; Liu et al. 2014; Nilsson et al. 2014; Schneider et al. 2021; Shang et al. 2021; Song et al. 2018; Sugiura et al. 2022; Yang et al. 2021; Yao et al. 2021; Yu et al. 2020).

Aberrant KRAS activity has been described previously to rewire the epigenetic regulation (Han et al. 2022; Kerk et al. 2021; Riquelme et al. 2016). Riquelme et al. (2016) showed that in $KRAS^{G12C}$ mutated NSCLC the expression of EZH2 was preferentially upregulated via the MEK-ERK signaling pathway, and EZH2 overexpression has been suggested to be inversely correlated with the prognosis in several human malignancies including NSCLC (Kim and Roberts 2016; Li et al. 2017; Riquelme et al. 2016; Shan et al. 2019; Wang et al. 2020; Yu et al. 2019; Zingg et al. 2015).

Based on the notion that KRAS plays a role in 1CM and epigenetic regulation, we investigated a cohort of 109 AC patients for the $KRAS^{G12C}$ mutation and the protein expression of MTHFD2 and EZH2. We found that the expression of both MTHFD2 and

EZH2 is increased in AC patients carrying KRAS-activating mutations. These results confirmed previous studies, where a positive correlation between MTHFD2/EZH2 expression and KRAS mutations in AC patients and cells has been shown (Fan et al. 2020; Moran et al. 2014; Riquelme et al. 2016). Further, our results revealed that high expression of MTHFD2 significantly correlated to both $KRAS^{G12C}$ and EZH2 expression. However, it remains to be established whether EZH2 promotes MTHFD2 expression. Importantly, only in KRAS-mutated cases, high expression of both MTHFD2 and EZH2 was predictive for inferior patient prognosis.

To investigate the expression and function of EZH2 and MTHFD2 in KRAS mutated cells, we used four AC cell lines. As expected, pharmacologic inhibition of KRAS with AMG510 suppressed the viability of cells and decreased MTHFD2 and EZH2 protein levels only in $KRAS^{G12C}$ cells. Further, the transient overexpression of G12C mutated $KRAS^{G12C}$ in the $KRAS^{WT}$ cell line H1993 verified the direct effect of KRAS activity on metabolism and the upregulation of MTHFD2 and EZH2 expression. Our finding not only shows a correlation between $KRAS^{G12C}$ and EZH2 expression but also indicates an important role in AC cellular viability. Ju et al have attempted to explain the mechanism of KRAS regulation of MTHFD2 in colon cancer by cellular myelocytomatosis oncogene (c-MYC) through phosphatidylinositol-4,5-bisphosphate 3-kinase (PI3K), protein kinase B (AKT) and extracellular signal regulated kinases (ERK) pathways (Boroughs and DeBerardinis 2015; Ju et al. 2019). Since our study shows a connection to EZH2, the regulatory mechanisms behind it are a matter of future investigation.

4.2 Correlation between EZH2 and MTHFD2 in AC

Several studies showed that epigenetic repression of EAF2-HIF1α by EZH2 fosters metabolic reprogramming in glioblastoma and promotes aerobic glycolysis by upregulating HK2 in prostate cancer (Pang et al. 2016; Tao et al. 2017). To study the function of EZH2 and the one-carbon metabolism enzyme MTHFD2 in vitro, specific knockdown revealed a $KRAS^{G12C}$-dependent MTHFD2 regulation by EZH2, whereas siRNAs against MTHFD2 did not affect EZH2 expression. We also show that a decreased cellular viability by pharmacological inhibition of KRAS is accompanied by reduced protein levels of MTHFD2 and EZH2 in $KRAS^{G12C}$ cells only. This was validated by the constitutive expression of aberrant KRAS in the $KRAS^{WT}$ cell line H1993 where metabolism, MTHFD2, and EZH2 expression were increased. This indicates that aberrant $KRAS^{G12C}$ activity is responsible for

the upregulation of MTHFD2 which is controlled by EZH2 methyltransferase activity. Our results show that the downregulation of MTHFD2 is a response to decreased EZH2 and suggests that this regulation most likely occurs indirectly. A possible mechanism would be that EZH2 targets an MTHFD2 transcriptional repressor. Moreover, 3D genome organization analyses showed that polycomb-bound loci form insulated and self-interacting chromatin domains (Li et al. 2018) and that the removal of EZH2 activity may play a key role in rewiring the MTHFD2 gene locus and impede the accession of its regulatory sequences. Polycomb marks are highly enriched at CpG islands (CGIs), and as known H3K27me3 distribution is negatively associated with DNA methylation, in this regard, the focus of EZH2 silenced close to the MTHFD2 gene may be DNA methylated (epigenetic switch) (Gal-Yam et al. 2008), leading to trigger the constitutive silencing of the entire locus in response to PRC repression inhibition.

There have also been indications that KRAS regulates MTHFD2 at a transcriptional level (Gal-Yam et al. 2008), but post-translational regulation seems also possible. One of the main mechanisms of MTHFD2 regulation is proteasomal degradation by acetylation (Almeida et al. 2021; Kawai et al. 2019). MTHFD2 is relatively low expressed in normal tissues (Li et al. 2018) and shows increased levels in multiple cancers, e. g. colorectal, breast, and hepatocellular cancers, where it plays an essential role in rewiring folate metabolism (Ferrai et al. 2017). Studies have shown that in breast cancer, acetylation of MTHFD2 by SIRT4 results in an enhanced proteasomal degradation (Almeida et al. 2021), and revealed that SIRT4 plays a protective role in cellular metabolism and serves as a sensor of folate availability. We show here that KRAS and EZH2 can enhance the metabolic state and folate availability, which may suggest that MTHFD2 is regulated by proteasomal degradation dependent on the cell's metabolic state.

4.3 Combining EZH2 and MTHFD2 inhibition in KRAS^{G12C} AC cells

Combination therapy is a common strategy in cancer treatment. Instead of using single drugs patients are treated with low doses of multiple treatments. The strategy of combining two or more FDA-approved therapies targeting the same pathway often not only ameliorates prognosis but also reduces side effects. This not only improves efficiency but also shortens the time required for approval, providing patients with timely and effective treatment. The specific EZH2 inhibitor GSK126 (Tazemetostat) was approved by the FDA in 2020 for the treatment of epithelioid sarcoma patients (Hoy 2020; Italiano 2020). AMG510 (Sotorasib)

against the $KRAS^{G12C}$ mutation was approved by FDA in 2021 as a second-line treatment for AC patients. DS18561882 is not yet in use but there is ongoing clinical trials (Mo et al. 2022). However, as long as DS18561882 is not approved we have to suggest DS18561882 as potentially therapeutic for AC To investigate combinational responses we used AMG510, GSK126, and DS18561882 in AC cells.

Strikingly, the inhibition of EZH2 or MTHFD2 strongly decreases cellular viability only in $KRAS^{G12C}$ cell lines. The increased response of $KRAS^{WT}$ cell line H1993 overexpressing $KRAS^{G12C}$ further underlined KRAS as the main driver of epigenetic regulation and increased 1CM activity in AC. These findings suggest that inhibition of EZH2 and MTHFD2 will be effective primarily against KRAS mutant AC. Targeting MTHFD2 and EZH2 has been suggested as therapeutic options for several solid tumors and lymphomas (Almeida et al. 2021; Hoy 2020; Italiano 2020; Ju et al. 2019; Kawai et al. 2019; Knutson et al. 2013; McCabe et al. 2012; Morschhauser et al. 2020). MTS cellular viability assay showed a strong and significant reduction of resistant cells' viability under the combined therapy (Bohnenberger et al. 2018).

To investigate the synergy of AMG510, GSK126, and DS18561882 we used the Chou-Talalay combination index (CI). Chou-Talalay is a method for calculating multiple drug interactions based on the median effect equation, which has been widely recognized and applied in recent years. It can be divided into synergistic, additive, and antagonistic effects represented by $CI < 1$, $CI = 1$, and $CI > 1$, respectively (Chou 2010). Importantly, here we show that co-targeting mutant KRAS and either EZH2 or MTHFD2 shows a synergistic effect in $KRAS^{G12C}$ cells ($CI < 1$) and, strikingly, the combined targeting of EZH2 and MTHFD2 had a similar synergistic effect as the combination treatment with AMG510. These findings strongly indicated that AC patients with a KRAS mutation other than $KRAS^{G12C}$ might also benefit from combined inhibition of MTHFD2 and EZH2.

Previous studies have shown that KRAS mutation rewired the metabolic network in multiple cancers through upregulating glycolytic activity (Ying et al. 2012). Others demonstrated that KRAS mutation and high expression of MTHFD2 induce cancer immune evasion through the PD-L1 up-regulation (Chen et al. 2017; Shang et al. 2021). Together with the observation that targeting cancer metabolism may synergistically enhance immunotherapy by reprogramming the tumor microenvironment (Li et al. 2019), co-targeting KRAS and either EZH2 or MTHFD2 might increase the efficacy of immunotherapeutic approaches in $KRAS^{MUT}$ AC patients. The co-inhibition of MTHFD2 and EZH2 in combination with

immunotherapy could be a treatment option for tumors with a KAS mutation other than $KRAS^{G12C}$. However, the efficacy and clinical application of MTHFD2 inhibitors in lung cancer still need further exploration.

4.4 Validation of the synergistic effect of inhibitors and PTX in cells

PTX is commonly used as first-line therapy for patients with driver gene-negative non-squamous NSCLC (Besse et al. 2014; Ettinger et al. 2022), as a novel anti-folate agent that inhibits THF cofactor-dependent enzymes (Chattopadhyay et al. 2007). Previous studies demonstrated that solid expression of MTHFD2 in KRAS mutant cells leads to a resistance of AC cells against PTX treatment. However, even though MTHFD2 was highly expressed in SQCLC and SCLC cell lines, cells responded well to PTX treatment (Yao et al. 2021). This suggested that AC cell lines may be particularly dependent on MTHFD2. Moreover, studies show that MTHFD2 expression was positively correlated with antifolate activity in KRAS mutant NSCLC cells (Moran et al. 2014).

Hence, to test whether PTX sensibility in HCC44 can be recovered by $KRAS^{G12C}$ inhibition, we assessed the expression of MTHFD2 after incubating HCC44 and H1993 cells with either AMG510, PTX or in combination. The combination of both agents almost entirely reduced MTHFD2 specifically in HCC44 but had nearly no effect on H1993. This indicated that pharmacologic inhibition of KRAS by AMG510 significantly improved PTX response in $KRAS^{MUT}$ cells. Importantly, we found that the combination treatment significantly reduced EZH2 expression, which was not achievable with monotherapy (Figure 22). We have provided evidence that AMG510 significantly reduces the $KRAS^{MUT}$ cell's metabolic state, thus increasing the PTX folic acid sensitivity. Besides, this also indicates that EZH2 plays a role in 1CM regulation and is also an important target for us to explore the mechanism of the 1CM network further.

Our analysis revealed a core resistance pathway to PTX inhibition in intrinsically resistant $KRAS^{MUT}$ AC cell lines. Selective inhibitors of AMG510, GSK126, and DS18561882 were used to inhibit KRAS, EZH2, and MTHFD2 in the resistant cell line HCC44 and the non-resistant cell line H1993. As expected, while the combination of PTX with AMG510, GSK126, or DS18561882 had no additional effect in the $KRAS^{WT}$ cell line H1993, we revealed a synergistic effect combining PTX with GSK126 or DS18561882 in the $KRAS^{G12C}$ cell line HCC44. As a combination therapy with PTX and AMG510 responded similarly to PTX treatment in the $KRAS^{WT}$ cells, we also recommend PTX as a treatment option for

$KRAS^{G12C}$ positive AC patients with a moderate response towards AMG510. Recently, Mo et al. (2022) also indicated that the combination of DS18561882 and Pemetrexed exhibited synergistic antitumor activity in lung cancer cells. DS18561882 has shown impressive therapeutic effects in preclinical models of multiple cancers, especially in AC cell lines, but it will take some time before clinical trials. In my study, the synergistic effect was similar when PTX was combined with DS18561882 or GSK126, which has already been approved for use in a variety of tumors (Hoy 2020). GSK126 combined with PTX is a promising treatment strategy improving the treatment efficacy in $KRAS^{MUT}$AC.

4.5 Conclusion

In the current thesis, I discovered a causal association between KRAS exon 2 mutation status and the expression of the epigenetic regulatory factor EZH2 and the 1CM key enzyme MTHFD2. KRAS-mutated AC cells are vulnerable to EZH2 and MTHFD2 inhibition by GSK126 and DS18561882 respectively, and combined treatment is as efficient as $KRAS^{G12C}$ inhibition with AMG510 alone. This reveals potential therapeutic options for resistant $KRAS^{G12C}$ and non-$KRAS^{G12C}$-mutated AC. In addition, we suggest that PTX also be a therapy option in AMG510-treated $KRAS^{G12C}$ AC with moderate response. These study results may lead to a more effective separation of AC patients and an improved response rate with combined therapy strategies (Figure 24).

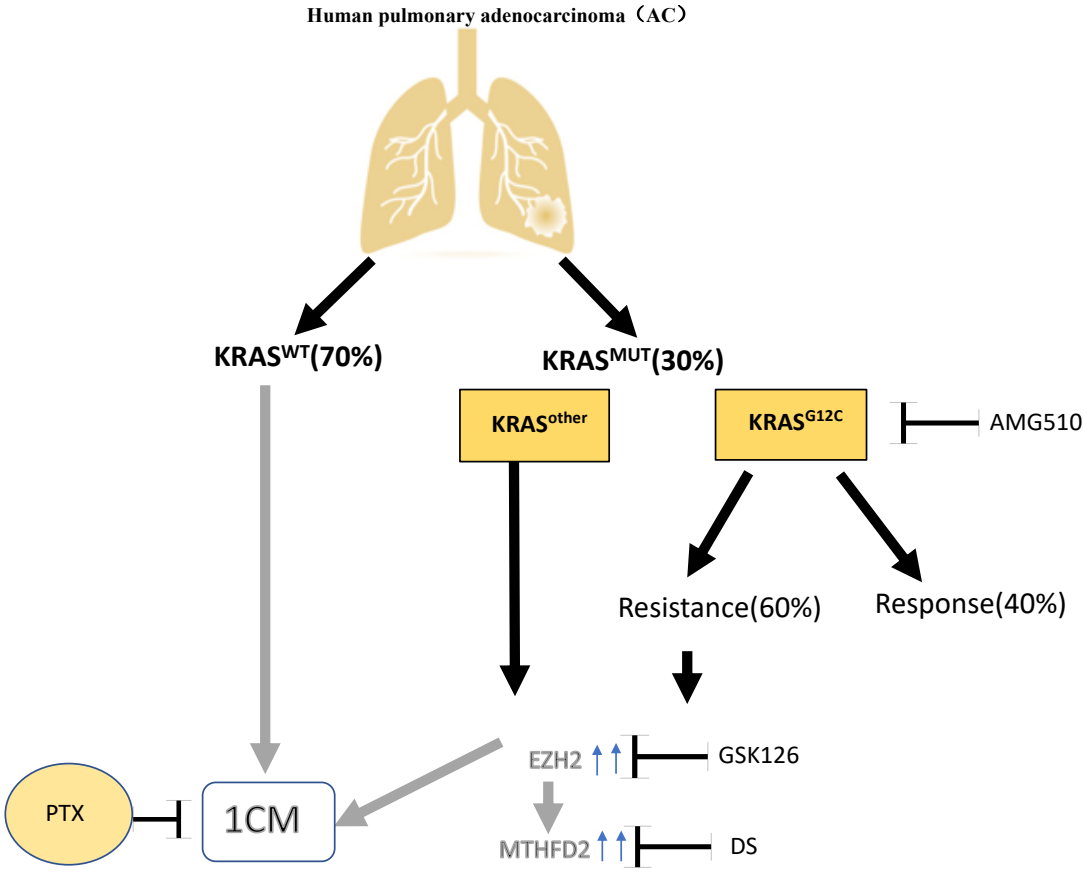

Figure 24: Hypothesised regulation and therapeutic targeting of MTHFD2, EZH2, and 1CM in KRAS mutated and WT AC.

5 Summary

With nearly 40 %, pulmonary adenocarcinomas are the main subgroup of non-small cell lung cancers. Activating KRAS mutations occur in about 30 % of pulmonary adenocarcinoma cases and the discovery of the G12C KRAS mutation-specific inhibitor Sotorasib has considerably improved patient prognosis. Despite the specificity, about 60 % of the patients carrying the G12C KRAS mutation are resistant to Sotorasib and different mutations still cannot be targeted. However, aberrant KRAS activity is also known to dysregulate one-carbon metabolism and epigenetic regulation. Though the mechanisms behind them are largely unknown, deciphering the interplay might lead to alternative and combinatorial treatments in KRAS aberrant and Sotorasib resistant patients. This thesis aimed to investigate the one-carbon metabolism factor MTHFD2 and the epigenetic regulator EZH2 in the context of KRAS exon 2 mutations in a cohort of pulmonary adenocarcinoma tissue samples and four pulmonary adenocarcinoma cell lines. We observed a KRAS mutation-dependent expression and prognostic relevance of MTHFD2 and EZH2 in pulmonary adenocarcinomas. In cell lines, an aberrant KRAS activity generated a vulnerability towards the MTHFD2 inhibitor DS18561882 and the EZH2 inhibitor GSK126. We found that combinational treatment with DS18561882 and GSK126 is synergistic and as effective as Sotorasib alone. The metabolic inhibitor pemetrexed in combination with DS18561882 or GSK126 also showed good activity in the G12C KRAS mutated cell lines and pemetrexed together with AMG510 even doubled the response. These observations open additional and alternative treatment combinations of aberrant KRAS-activated pulmonary adenocarcinomas.

6 References

Addeo A, Tabbò F, Robinson T, Buffoni L, Novello S (2018): Precision medicine in ALK rearranged NSCLC: A rapidly evolving scenario. Crit Rev Oncol Hematol 122, 150-156

Almeida L, Dhillon-LaBrooy A, Castro CN, Adossa N, Carriche GM, Guderian M, Lippens S, Dennerlein S, Hesse C, Lambrecht BN, et al. (2021): Ribosome-Targeting Antibiotics Impair T Cell Effector Function and Ameliorate Autoimmunity by Blocking Mitochondrial Protein Synthesis. Immunity 54, 68-83.e66

Ben-Sahra I, Hoxhaj G, Ricoult SJH, Asara JM, Manning BD (2016): mTORC1 induces purine synthesis through control of the mitochondrial tetrahydrofolate cycle. Science 351, 728-733

Besse B, Adjei A, Baas P, Meldgaard P, Nicolson M, Paz-Ares L, Reck M, Smit EF, Syrigos K, Stahel R, et al. (2014): 2nd ESMO Consensus Conference on Lung Cancer: non-small-cell lung cancer first-line/second and further lines of treatment in advanced disease. Ann Oncol 25, 1475-1484

Bohnenberger H, Kaderali L, Ströbel P, Yepes D, Plessmann U, Dharia NV, Yao S, Heydt C, Merkelbach-Bruse S, Emmert A, et al. (2018): Comparative proteomics reveals a diagnostic signature for pulmonary head-and-neck cancer metastasis. EMBO Mol Med 10, e8428

Bonagas N, Gustafsson NMS, Henriksson M, Marttila P, Gustafsson R, Wiita E, Borhade S, Green AC, Vallin KSA, Sarno A, et al. (2022): Pharmacological targeting of MTHFD2 suppresses acute myeloid leukemia by inducing thymidine depletion and replication stress. Nat Cancer 3, 156-172

Boroughs LK, DeBerardinis RJ (2015): Metabolic pathways promoting cancer cell survival and growth. Nat Cell Biol 17, 351-359

Bremer SCB, Conradi LC, Mechie NC, Amanzada A, Mavropoulou E, Kitz J, Ghadimi M, Ellenrieder V, Ströbel P, Hessmann E, et al. (2021): Enhancer of Zeste Homolog 2 in Colorectal Cancer Development and Progression. Digestion 102, 227-235

Brenner DR, Yannitsos DH, Farris MS, Johansson M, Friedenreich CM (2016): Leisure-time physical activity and lung cancer risk: A systematic review and meta-analysis. Lung Cancer 95, 17-27

Brenner DR, Boffetta P, Duell EJ, Bickeböller H, Rosenberger A, McCormack V, Muscat JE, Yang P, Wichmann HE, Brueske-Hohlfeld I, et al. (2012): Previous lung diseases and lung cancer risk: a pooled analysis from the International Lung Cancer Consortium. Am J Epidemiol 176, 573-585

Cancer Genome Atlas Research Network (2014): Comprehensive molecular profiling of lung adenocarcinoma. Nature 511, 543-550

Chaft JE, Rimner A, Weder W, Azzoli CG, Kris MG, Cascone T (2021): Evolution of systemic therapy for stages I-III non-metastatic non-small-cell lung cancer. Nat Rev Clin Oncol 18, 547-557

Chattopadhyay S, Moran RG, Goldman ID (2007): Pemetrexed: biochemical and cellular pharmacology, mechanisms, and clinical applications. Mol Cancer Ther 6, 404-417

Chen N, Fang W, Lin Z, Peng P, Wang J, Zhan J, Hong S, Huang J, Liu L, Sheng J, et al. (2017): KRAS mutation-induced upregulation of PD-L1 mediates immune escape in human lung adenocarcinoma. Cancer Immunol Immunother 66, 1175-1187

Cho KR, Vogelstein B (1992): Genetic alterations in the adenoma--carcinoma sequence. Cancer 70, 1727-1731

Chou TC (2010): Drug combination studies and their synergy quantification using the Chou-Talalay method. Cancer Res 70, 440-446

Christensen KE, MacKenzie RE (2006): Mitochondrial one-carbon metabolism is adapted to the specific needs of yeast, plants and mammals. Bioessays 28, 595-605

Ducker GS, Rabinowitz JD (2017): One-Carbon Metabolism in Health and Disease. Cell Metab 25, 27-42

Duruisseaux M, Esteller M (2018): Lung cancer epigenetics: From knowledge to applications. Semin Cancer Biol 51, 116-128

El Osta B, Behera M, Kim S, Berry LD, Sica G, Pillai RN, Owonikoko TK, Kris MG, Johnson BE, Kwiatkowski DJ, et al. (2019): Characteristics and Outcomes of Patients With Metastatic KRAS-Mutant Lung Adenocarcinomas: The Lung Cancer Mutation Consortium Experience. J Thorac Oncol 14, 876-889

Ettinger DS, Wood DE, Aisner DL, Akerley W, Bauman JR, Bharat A, Bruno DS, Chang JY, Chirieac LR, D'Amico TA, et al. (2022): Non-Small Cell Lung Cancer, Version 3.2022, NCCN Clinical Practice Guidelines in Oncology. J Natl Compr Canc Netw 20, 497-530

Fan K, Zhang CL, Qi YF, Dai X, Birling Y, Tan ZF, Cao F (2020): Prognostic Value of EZH2 in Non-Small-Cell Lung Cancers: A Meta-Analysis and Bioinformatics Analysis. Biomed Res Int 2020, 2380124

Ferrai C, Torlai Triglia E, Risner-Janiczek JR, Rito T, Rackham OJ, de Santiago I, Kukalev A, Nicodemi M, Akalin A, Li M, et al. (2017): RNA polymerase II primes Polycomb-repressed developmental genes throughout terminal neuronal differentiation. Mol Syst Biol 13, 946

Friedlaender A, Banna G, Patel S, Addeo A (2019): Diagnosis and Treatment of ALK Aberrations in Metastatic NSCLC. Curr Treat Options Oncol 20, 79

Friedlaender A, Drilon A, Weiss GJ, Banna GL, Addeo A (2020): KRAS as a druggable target in NSCLC: Rising like a phoenix after decades of development failures. Cancer Treat Rev 85, 101978

Frisone D, Friedlaender A, Malapelle U, Banna G, Addeo A (2020): A BRAF new world. Crit Rev Oncol Hematol 152, 103008

Fujimoto A, Furuta M, Totoki Y, Tsunoda T, Kato M, Shiraishi Y, Tanaka H, Taniguchi H, Kawakami Y, Ueno M, et al. (2016): Whole-genome mutational landscape and characterization of noncoding and structural mutations in liver cancer. Nat Genet 48, 500-509

Gal-Yam EN, Egger G, Iniguez L, Holster H, Einarsson S, Zhang X, Lin JC, Liang G, Jones PA, Tanay A (2008): Frequent switching of Polycomb repressive marks and DNA hypermethylation in the PC3 prostate cancer cell line. Proc Natl Acad Sci U S A 105, 12979-12984

Guibert N, Ilie M, Long E, Hofman V, Bouhlel L, Brest P, Mograbi B, Marquette CH, Didier A, Mazieres J, et al. (2015): KRAS Mutations in Lung Adenocarcinoma: Molecular and Epidemiological Characteristics, Methods for Detection, and Therapeutic Strategy Perspectives. Curr Mol Med 15, 418-432

Han Z, Zhou D, Wang J, Jiang B, Liu X (2022): Reflections on drug resistance to KRAS(G12C) inhibitors and gene silencing/editing tools for targeting mutant KRAS in cancer treatment. Biochim Biophys Acta Rev Cancer 1877, 188677

Hanahan D, Weinberg RA (2011): Hallmarks of cancer: the next generation. Cell 144, 646-674

Hecht SS (1999): Tobacco smoke carcinogens and lung cancer. J Natl Cancer Inst 91, 1194-1210

Hong DS, Fakih MG, Strickler JH, Desai J, Durm GA, Shapiro GI, Falchook GS, Price TJ, Sacher A, Denlinger CS, et al. (2020): KRAS(G12C) Inhibition with Sotorasib in Advanced Solid Tumors. N Engl J Med 383, 1207-1217

Hoy SM (2020): Tazemetostat: First Approval. Drugs 80, 513-521

Hu S, Yu L, Li Z, Shen Y, Wang J, Cai J, Xiao L, Wang Z (2010): Overexpression of EZH2 contributes to acquired cisplatin resistance in ovarian cancer cells in vitro and in vivo. Cancer Biol Ther 10, 788-795

Italiano A (2020): Targeting epigenetics in sarcomas through EZH2 inhibition. J Hematol Oncol 13, 33

Jänne PA, Riely GJ, Gadgeel SM, Heist RS, Ou SI, Pacheco JM, Johnson ML, Sabari JK, Leventakos K, Yau E, et al. (2022): Adagrasib in Non-Small-Cell Lung Cancer Harboring a KRAS(G12C) Mutation. N Engl J Med 387, 120-131

Ju HQ, Lu YX, Chen DL, Zuo ZX, Liu ZX, Wu QN, Mo HY, Wang ZX, Wang DS, Pu HY, et al. (2019): Modulation of Redox Homeostasis by Inhibition of MTHFD2 in Colorectal Cancer: Mechanisms and Therapeutic Implications. J Natl Cancer Inst 111, 584-596

Kaelin WG, Jr., Thompson CB (2010): Q&A: Cancer: clues from cell metabolism. Nature 465, 562-564

Kalemkerian GP, Narula N, Kennedy EB, Biermann WA, Donington J, Leighl NB, Lew M, Pantelas J, Ramalingam SS, Reck M, et al. (2018): Molecular Testing Guideline for the Selection of Patients With Lung Cancer for Treatment With Targeted Tyrosine Kinase Inhibitors: American Society of Clinical Oncology Endorsement of the College of American Pathologists/International Association for the Study of Lung Cancer/Association for Molecular Pathology Clinical Practice Guideline Update. J Clin Oncol 36, 911-919

Kawai J, Toki T, Ota M, Inoue H, Takata Y, Asahi T, Suzuki M, Shimada T, Ono K, Suzuki K, et al. (2019): Discovery of a Potent, Selective, and Orally Available MTHFD2 Inhibitor (DS18561882) with in Vivo Antitumor Activity. J Med Chem 62, 10204-10220

Kerk SA, Papagiannakopoulos T, Shah YM, Lyssiotis CA (2021): Metabolic networks in mutant KRAS-driven tumours: tissue specificities and the microenvironment. Nat Rev Cancer 21, 510-525

Kim CH, Lee YC, Hung RJ, Boffetta P, Xie D, Wampfler JA, Cote ML, Chang SC, Ugolini D, Neri M, et al. (2015): Secondhand Tobacco Smoke Exposure and Lung Adenocarcinoma In Situ/Minimally Invasive Adenocarcinoma (AIS/MIA). Cancer Epidemiol Biomarkers Prev 24, 1902-1906

Kim KH, Roberts CW (2016): Targeting EZH2 in cancer. Nat Med 22, 128-134

Knutson SK, Warholic NM, Wigle TJ, Klaus CR, Allain CJ, Raimondi A, Porter Scott M, Chesworth R, Moyer MP, Copeland RA, et al. (2013): Durable tumor regression in genetically altered malignant rhabdoid tumors by inhibition of methyltransferase EZH2. Proc Natl Acad Sci U S A 110, 7922-7927

Li B, Huang Z, Yu W, Liu S, Zhang J, Wang Q, Wu L, Kou F, Yang L (2021): Molecular subtypes based on CNVs related gene signatures identify candidate prognostic biomarkers in lung adenocarcinoma. Neoplasia 23, 704-717

Li X, Wenes M, Romero P, Huang SC, Fendt SM, Ho PC (2019): Navigating metabolic pathways to enhance antitumour immunity and immunotherapy. Nat Rev Clin Oncol 16, 425-441

Li Y, Elakad O, Yao S, von Hammerstein-Equord A, Hinterthaner M, Danner BC, Ferrai C, Ströbel P, Küffer S, Bohnenberger H (2022): Regulation and Therapeutic Targeting of MTHFD2 and EZH2 in KRAS-Mutated Human Pulmonary Adenocarcinoma. Metabolites 12, 652

Li Y, Zheng H, Wang Q, Zhou C, Wei L, Liu X, Zhang W, Zhang Y, Du Z, Wang X, et al. (2018): Genome-wide analyses reveal a role of Polycomb in promoting hypomethylation of DNA methylation valleys. Genome Biol 19, 18

Li Z, Hou P, Fan D, Dong M, Ma M, Li H, Yao R, Li Y, Wang G, Geng P, et al. (2017): The degradation of EZH2 mediated by lncRNA ANCR attenuated the invasion and metastasis of breast cancer. Cell Death Differ 24, 59-71

Lindeman NI, Cagle PT, Beasley MB, Chitale DA, Dacic S, Giaccone G, Jenkins RB, Kwiatkowski DJ, Saldivar JS, Squire J, et al. (2013): Molecular testing guideline for selection of lung cancer patients for EGFR and ALK tyrosine kinase inhibitors: guideline from the College of American Pathologists, International Association for the Study of Lung Cancer, and Association for Molecular Pathology. J Thorac Oncol 8, 823-859

Liu F, Liu Y, He C, Tao L, He X, Song H, Zhang G (2014): Increased MTHFD2 expression is associated with poor prognosis in breast cancer. Tumour Biol 35, 8685-8690

McCabe MT, Ott HM, Ganji G, Korenchuk S, Thompson C, Van Aller GS, Liu Y, Graves AP, Della Pietra A, 3rd, Diaz E, et al. (2012): EZH2 inhibition as a therapeutic strategy for lymphoma with EZH2-activating mutations. Nature 492, 108-112

Mo J, Gao Z, Zheng L, Yan M, Xue M, Xu J, Bao Y, Wu J (2022): Targeting mitochondrial one-carbon enzyme MTHFD2 together with pemetrexed confers therapeutic advantages in lung adenocarcinoma. Cell Death Discov 8, 307

Moran DM, Trusk PB, Pry K, Paz K, Sidransky D, Bacus SS (2014): KRAS mutation status is associated with enhanced dependency on folate metabolism pathways in non-small cell lung cancer cells. Mol Cancer Ther 13, 1611-1624

Morschhauser F, Tilly H, Chaidos A, McKay P, Phillips T, Assouline S, Batlevi CL, Campbell P, Ribrag V, Damaj GL, et al. (2020): Tazemetostat for patients with relapsed or refractory follicular lymphoma: an open-label, single-arm, multicentre, phase 2 trial. Lancet Oncol 21, 1433-1442

Nakajima EC, Drezner N, Li X, Mishra-Kalyani PS, Liu Y, Zhao H, Bi Y, Liu J, Rahman A, Wearne E, et al. (2022): FDA Approval Summary: Sotorasib for KRAS G12C-Mutated Metastatic NSCLC. Clin Cancer Res 28, 1482-1486

Nilsson R, Jain M, Madhusudhan N, Sheppard NG, Strittmatter L, Kampf C, Huang J, Asplund A, Mootha VK (2014): Metabolic enzyme expression highlights a key role for MTHFD2 and the mitochondrial folate pathway in cancer. Nat Commun 5, 3128

Öberg M, Jaakkola MS, Woodward A, Peruga A, Prüss-Ustün A (2011): Worldwide burden of disease from exposure to second-hand smoke: a retrospective analysis of data from 192 countries. Lancet 377, 139-146

Pan Y, Zhang Y, Ye T, Zhao Y, Gao Z, Yuan H, Zheng D, Zheng S, Li H, Li Y, et al. (2019): Detection of Novel NRG1, EGFR, and MET Fusions in Lung Adenocarcinomas in the Chinese Population. J Thorac Oncol 14, 2003-2008

Pang B, Zheng XR, Tian JX, Gao TH, Gu GY, Zhang R, Fu YB, Pang Q, Li XG, Liu Q (2016): EZH2 promotes metabolic reprogramming in glioblastomas through epigenetic repression of EAF2-HIF1α signaling. Oncotarget 7, 45134-45143

Planchard D, Smit EF, Groen HJM, Mazieres J, Besse B, Helland Å, Giannone V, D'Amelio AM, Jr., Zhang P, Mookerjee B, et al. (2017): Dabrafenib plus trametinib in patients with previously untreated BRAF(V600E)-mutant metastatic non-small-cell lung cancer: an open-label, phase 2 trial. Lancet Oncol 18, 1307-1316

Planchard D, Besse B, Groen HJM, Souquet PJ, Quoix E, Baik CS, Barlesi F, Kim TM, Mazieres J, Novello S, et al. (2016): Dabrafenib plus trametinib in patients with previously treated BRAF(V600E)-mutant metastatic non-small cell lung cancer: an open-label, multicentre phase 2 trial. Lancet Oncol 17, 984-993

Riquelme E, Behrens C, Lin HY, Simon G, Papadimitrakopoulou V, Izzo J, Moran C, Kalhor N, Lee JJ, Minna JD, et al. (2016): Modulation of EZH2 Expression by MEK-ERK or PI3K-

AKT Signaling in Lung Cancer Is Dictated by Different KRAS Oncogene Mutations. Cancer Res 76, 675-685

Rodriguez-Canales J, Parra-Cuentas E, Wistuba, II (2016): Diagnosis and Molecular Classification of Lung Cancer. Cancer Treat Res 170, 25-46

Saliani M, Mirzaiebadizi A, Javadmanesh A, Siavoshi A, Ahmadian MR (2022): KRAS-related long noncoding RNAs in human cancers. Cancer Gene Ther 29, 418-427

Schneider CA, Rasband WS, Eliceiri KW (2012): NIH Image to ImageJ: 25 years of image analysis. Nat Methods 9, 671-675

Schneider G, Wirth M, Keller U, Saur D (2021): Rationale for MYC imaging and targeting in pancreatic cancer. EJNMMI Res 11, 104

Schwartz AG, Cote ML (2016): Epidemiology of Lung Cancer. Adv Exp Med Biol 893, 21-41

Sequist LV, Yang JC, Yamamoto N, O'Byrne K, Hirsh V, Mok T, Geater SL, Orlov S, Tsai CM, Boyer M, et al. (2013): Phase III study of afatinib or cisplatin plus pemetrexed in patients with metastatic lung adenocarcinoma with EGFR mutations. J Clin Oncol 31, 3327-3334

Shan J, Al-Muftah MA, Al-Kowari MK, Abuaqel SWJ, Al-Rumaihi K, Al-Bozom I, Li P, Chouchane L (2019): Targeting Wnt/EZH2/microRNA-708 signaling pathway inhibits neuroendocrine differentiation in prostate cancer. Cell Death Discov 5, 139

Shang M, Yang H, Yang R, Chen T, Fu Y, Li Y, Fang X, Zhang K, Zhang J, Li H, et al. (2021): The folate cycle enzyme MTHFD2 induces cancer immune evasion through PD-L1 up-regulation. Nat Commun 12, 1940

Skoulidis F, Li BT, Dy GK, Price TJ, Falchook GS, Wolf J, Italiano A, Schuler M, Borghaei H, Barlesi F, et al. (2021): Sotorasib for Lung Cancers with KRAS p.G12C Mutation. N Engl J Med 384, 2371-2381

Smith HW, Hirukawa A, Sanguin-Gendreau V, Nandi I, Dufour CR, Zuo D, Tandoc K, Leibovitch M, Singh S, Rennhack JP, et al. (2019): An ErbB2/c-Src axis links bioenergetics with PRC2 translation to drive epigenetic reprogramming and mammary tumorigenesis. Nat Commun 10, 2901

Song Z, Feng C, Lu Y, Lin Y, Dong C (2018): PHGDH is an independent prognosis marker and contributes cell proliferation, migration and invasion in human pancreatic cancer. Gene 642, 43-50

Stine ZE, Schug ZT, Salvino JM, Dang CV (2022): Targeting cancer metabolism in the era of precision oncology. Nat Rev Drug Discov 21, 141-162

Sugiura A, Andrejeva G, Voss K, Heintzman DR, Xu X, Madden MZ, Ye X, Beier KL, Chowdhury NU, Wolf MM, et al. (2022): MTHFD2 is a metabolic checkpoint controlling effector and regulatory T cell fate and function. Immunity 55, 65-81.e69

Sung H, Ferlay J, Siegel RL, Laversanne M, Soerjomataram I, Jemal A, Bray F (2021): Global Cancer Statistics 2020: GLOBOCAN Estimates of Incidence and Mortality Worldwide for 36 Cancers in 185 Countries. CA Cancer J Clin 71, 209-249

Tao S, Wang S, Moghaddam SJ, Ooi A, Chapman E, Wong PK, Zhang DD (2014): Oncogenic KRAS confers chemoresistance by upregulating NRF2. Cancer Res 74, 7430-7441

Tao T, Chen M, Jiang R, Guan H, Huang Y, Su H, Hu Q, Han X, Xiao J (2017): Involvement of EZH2 in aerobic glycolysis of prostate cancer through miR-181b/HK2 axis. Oncol Rep 37, 1430-1436

Travis WD, Brambilla E, Nicholson AG, Yatabe Y, Austin JHM, Beasley MB, Chirieac LR, Dacic S, Duhig E, Flieder DB, et al. (2015): The 2015 World Health Organization Classification of Lung Tumors: Impact of Genetic, Clinical and Radiologic Advances Since the 2004 Classification. J Thorac Oncol 10, 1243-1260

Turner MC, Chen Y, Krewski D, Calle EE, Thun MJ (2007): Chronic obstructive pulmonary disease is associated with lung cancer mortality in a prospective study of never smokers. Am J Respir Crit Care Med 176, 285-290

Wang H, Su H, Tan Y (2020): UNC5B-AS1 promoted ovarian cancer progression by regulating the H3K27me on NDRG2 via EZH2. Cell Biol Int 44, 1028-1036

Weller M, Weber RG, Willscher E, Riehmer V, Hentschel B, Kreuz M, Felsberg J, Beyer U, Löffler-Wirth H, Kaulich K, et al. (2015): Molecular classification of diffuse cerebral WHO grade II/III gliomas using genome- and transcriptome-wide profiling improves stratification of prognostically distinct patient groups. Acta Neuropathol 129, 679-693

Wistuba, II, Behrens C, Milchgrub S, Bryant D, Hung J, Minna JD, Gazdar AF (1999): Sequential molecular abnormalities are involved in the multistage development of squamous cell lung carcinoma. Oncogene 18, 643-650

Woo HG, Choi JH, Yoon S, Jee BA, Cho EJ, Lee JH, Yu SJ, Yoon JH, Yi NJ, Lee KW, et al. (2017): Integrative analysis of genomic and epigenomic regulation of the transcriptome in liver cancer. Nat Commun 8, 839

World Medical Association (2013): World Medical Association Declaration of Helsinki: ethical principles for medical research involving human subjects. JAMA 310, 2191-2194

Xu W, Xu M, Wang L, Zhou W, Xiang R, Shi Y, Zhang Y, Piao Y (2019): Integrative analysis of DNA methylation and gene expression identified cervical cancer-specific diagnostic biomarkers. Signal Transduct Target Ther 4, 55

Yang C, Zhang J, Liao M, Yang Y, Wang Y, Yuan Y, Ouyang L (2021): Folate-mediated one-carbon metabolism: a targeting strategy in cancer therapy. Drug Discov Today 26, 817-825

Yang J, Ren B, Yang G, Wang H, Chen G, You L, Zhang T, Zhao Y (2020): The enhancement of glycolysis regulates pancreatic cancer metastasis. Cell Mol Life Sci 77, 305-321

Yao S, Peng L, Elakad O, Küffer S, Hinterthaner M, Danner BC, von Hammerstein-Equord A, Ströbel P, Bohnenberger H (2021): One carbon metabolism in human lung cancer. Transl Lung Cancer Res 10, 2523-2538

Ying H, Kimmelman AC, Lyssiotis CA, Hua S, Chu GC, Fletcher-Sananikone E, Locasale JW, Son J, Zhang H, Coloff JL, et al. (2012): Oncogenic Kras maintains pancreatic tumors through regulation of anabolic glucose metabolism. Cell 149, 656-670

Yu C, Yang L, Cai M, Zhou F, Xiao S, Li Y, Wan T, Cheng D, Wang L, Zhao C, et al. (2020): Down-regulation of MTHFD2 inhibits NSCLC progression by suppressing cycle-related genes. J Cell Mol Med 24, 1568-1577

Yu HA, Arcila ME, Rekhtman N, Sima CS, Zakowski MF, Pao W, Kris MG, Miller VA, Ladanyi M, Riely GJ (2013): Analysis of tumor specimens at the time of acquired resistance to EGFR-TKI therapy in 155 patients with EGFR-mutant lung cancers. Clin Cancer Res 19, 2240-2247

Yu Y, Qi J, Xiong J, Jiang L, Cui D, He J, Chen P, Li L, Wu C, Ma T, et al. (2019): Epigenetic Co-Deregulation of EZH2/TET1 is a Senescence-Countering, Actionable Vulnerability in Triple-Negative Breast Cancer. Theranostics 9, 761-777

Yuan TL, Amzallag A, Bagni R, Yi M, Afghani S, Burgan W, Fer N, Strathern LA, Powell K, Smith B, et al. (2018): Differential Effector Engagement by Oncogenic KRAS. Cell Rep 22, 1889-1902

Zheng M (2016): Classification and Pathology of Lung Cancer. Surg Oncol Clin N Am 25, 447-468

Zheng X, Luo J, Liu W, Ashby CR, Jr., Chen ZS, Lin L (2022): Sotorasib: a treatment for non-small cell lung cancer with the KRAS G12C mutation. Drugs Today (Barc) 58, 175-185

Zhou Y, Tozzi F, Chen J, Fan F, Xia L, Wang J, Gao G, Zhang A, Xia X, Brasher H, et al. (2012): Intracellular ATP levels are a pivotal determinant of chemoresistance in colon cancer cells. Cancer Res 72, 304-314

Zingg D, Debbache J, Schaefer SM, Tuncer E, Frommel SC, Cheng P, Arenas-Ramirez N, Haeusel J, Zhang Y, Bonalli M, et al. (2015): The epigenetic modifier EZH2 controls melanoma growth and metastasis through silencing of distinct tumour suppressors. Nat Commun 6, 6051

ACKNOWLEDGEMENTS

I would like to show my gratitude to Prof. Dr. med. Philipp Ströbel and PD Dr. med. Alexander von Hammerstein-Equord for supervising me on this exciting topic in Göttingen, the professional working environment created throughout the research process, and the continuous support of my project and research.

I sincerely thank Dr. med. Hanibal Bohnenberger for his continuous support and shining advice that helped to overcome difficulties. His diligent, pragmatic, and responsible work inspired me to become a scientist in academic and experimental work.

I am grateful to Dr. sc. hum. Stefan Küffer for his guidance, encouragement, and helpful discussion during the experiments. Whenever I met difficulties, he could always come up with constructive ideas and practical suggestions and guided me to form more rigorous logical thinking in scientific research.

I am very grateful for the tremendous help and support I received from Dr. rer. nat. Omar Elakad.

Thanks for everything!